NASA CONTRACTOR REPORT

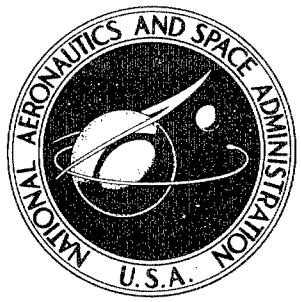

NASA CR-985

NASA CR-985

STUDY OF VIBRATION MEASUREMENT BY LASER METHODS

by Gail A. Massey

Prepared by
SYLVANIA ELECTRONIC SYSTEMS
Mountain View, Calif.
for Ames Research Center

NATIONAL AERONAUTICS AND SPACE ADMINISTRATION • WASHINGTON, D. C. • JANUARY 1968

NASA CR-985

STUDY OF VIBRATION MEASUREMENT BY LASER METHODS

By Gail A. Massey

Prepared under Contract No. NAS 2-3643 by
SYLVANIA ELECTRONIC SYSTEMS
Mountain View, Calif.

for Ames Research Center

NATIONAL AERONAUTICS AND SPACE ADMINISTRATION

For sale by the Clearinghouse for Federal Scientific and Technical Information
Springfield, Virginia 22151 – CFSTI price $3.00

TABLE OF CONTENTS

LIST OF ILLUSTRATIONS

STUDY OF VIBRATION MEASUREMENT BY LASER METHODS

By G. A. Massey
Sylvania Electronic Systems

SUMMARY

This report describes results of the second phase of a study of techniques for using laser radiation to detect and measure vibration of mechanical structures. During the first study phase, a number of methods were suggested and demonstrated; two of these were selected as sufficiently promising to merit further investigation. One of these methods is the intermediate frequency optical heterodyne system, which provides quantitative data about the motion of a particular very small area on the mechanical structure. The other method is a qualitative interference technique for observing the vibrational mode patterns, so that the number of points to be measured by other methods can be reduced. During the second study phase, these two methods have been developed analytically and experimentally. A breadboard optical heterodyne system was built, and detection of audio frequency vibrations at levels from one centimeter to less than 0.1 micron peak-to-peak has been achieved with a variety of surface materials. The performance of this system using two different types of demodulation circuits was investigated in detail. A model structure was fabricated for tests involving comparisons of the qualitative and quantitative methods. It has been shown that a very good knowledge of the vibrational modes can be obtained using the two methods in combination. The qualitative interference method also has been extended to include the measurement of axes of rotation.

INTRODUCTION

This report describes the work performed during a six-month study sponsored by the National Aeronautics and Space Administration, Ames Research Center. The purpose of this study was to investigate and develop methods for employing optical devices to measure vibrations of a mechanical structure. In particular, the novel techniques made possible by laser sources of great spatial and spectral coherence have been investigated. Since other devices for vibration analysis are already in use and have been developed extensively, it is reasonable to ask whether laser measuring systems offer any advantages over the older methods. There are, in fact, a number of important advantages, some of which are listed below.

(1) Measurements can be made without attaching any mass to the structure.

(2) The working distance between the structure and the test instrument is limited only by source power and the maximum size of the optical system that is tolerable.

(3) The area over which the measurement is made can be variable and may be small, since the optical beam can be focused.

(4) The frequency response is not limited by resonances such as those present in mechanical strain gauges or accelerometers.

(5) The sensitivity to small motion is, at least for some of the optical systems proposed, much better than most applications require as a minimum.

During a previous study, several methods were investigated. These systems included interferometric methods, high-frequency subcarrier modulation systems, and radiometric devices sensitive to image motion. Of these techniques, two were selected for further study because initial tests were highly successful.

INTERMEDIATE FREQUENCY OPTICAL HETERODYNE SYSTEM

The intermediate frequency heterodyne system was selected during the previous study as the most versatile and sensitive quantitative measurement technique. In this scheme the laser output beam is divided into two parts. One part is transmitted to the vibrating surface through the optical system of the instrument. The other is shifted in frequency by an amount (in the present experiments approximately 15 MHz) large compared to the expected Doppler shifts on the reflected light from the surface under measurement. The shifted beam is sent to a beamsplitter mirror and from there directly into the photodetector; this beam is known as the reference or local oscillator beam. Some of the reflected light from the moving surface returns through the instrument optical system and is combined with the reference beam at the beamsplitter. A block diagram of this system is shown in Figure 1. Interference between the reference and signal beams is thus produced on the photodetector. A stationary surface produces interference which varies sinusoidally at the difference frequency, which is just equal to the shift or system intermediate frequency (IF). If the surface moves, the phase or frequency of the interference changes, producing frequency modulation of the system IF. The shift provides a frequency "bias" so that motions toward or away from the instrument produce distinctive Doppler modulations which give the motion direction as well as magnitude. The processing of the electronic signal from the detector is therefore relatively straightforward. For reference purposes, an analysis of the heterodyne detection process is presented next.

General Analysis of Heterodyne Detection

The optical electric fields present on the square-law photodetector are $E_S \cos(\omega_o' t + \phi_S)$, due to reflected optical signal, and $E_{LO} \cos(\omega_o t + \phi_{LO})$

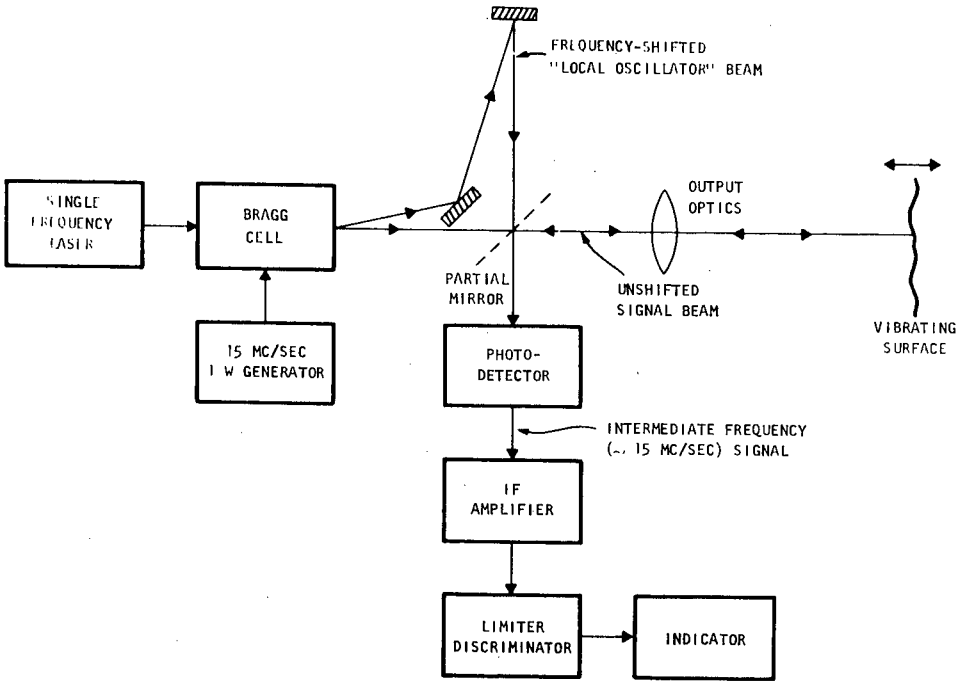

Figure 1. Block Diagram, Intermediate Frequency System.

from the local oscillator beam. The detector responds with a current proportional to the square of the resultant field, or:

$$i(t) \sim \left[E_S \cos(\omega_o' t + \phi_S) + E_{LO} \cos(\omega_o t + \phi_{LO})\right]^2$$

$$= E_S^2 \cos^2(\omega_o' t + \phi_S) + E_{LO}^2 \cos^2(\omega_o t + \phi_{LO})$$

$$+ 2 E_S E_{LO} \cos(\omega_o' t + \phi_S) \cos(\omega_o t + \phi_{LO})$$

$$= \frac{E_S^2}{2} + \frac{E_{LO}^2}{2} + \frac{E_S}{2} \cos 2(\omega_o' t + \phi_S) + \frac{E_{LO}}{2} \cos 2(\omega_o t + \phi_{LO})$$

$$+ E_S E_{LO} \cos\left[(\omega_o' + \omega_o)t + \phi_S + \phi_{LO}\right]$$

$$+ E_S E_{LO} \cos\left[(\omega_o' - \omega_o)t + \phi_S - \phi_{LO}\right] .$$

The third, fourth, and fifth terms of this expression are at optical frequencies and thus average to zero. This leaves an expression for the current of the form:

$$i(t) = I_{LO} + I_S + 2\sqrt{I_{LO} I_S} \cos\left[\omega t + \phi_S - \phi_{LO}\right]$$

where I_{LO} and I_S are the dc currents produced by the local oscillator and signal beams alone, and the interference term has a frequency ω equal to the shift frequency or system IF. The local oscillator phase is constant, depending only on the arbitrary choice of time reference; hence it can be set equal to zero. The signal phase ϕ_S varies with time such that for a sinusoidal vibration:

$$\phi_S = \frac{4\pi x_o}{\lambda} \sin \omega_v t ,$$

where x_o is the peak vibration amplitude, ω_v is the vibration frequency, and λ is the laser wavelength. This can be interpreted also as a frequency modulation by taking the time derivative of the phase:

$$\Delta\omega(t) = \frac{d\phi_S}{dt} = \frac{4\pi x_o \omega_v}{\lambda} \cos \omega_v t \qquad \text{(radians per second)}$$

or

$$\Delta f(t) = \frac{1}{2\pi} \Delta\omega(t) = \frac{2x_o \omega_v}{\lambda} \cos\omega_v t \qquad \text{(cycles per second)}$$

Therefore the ac component of the photodetector current is given by:

$$i_{ac} = 2\sqrt{I_{LO} I_S} \cos\left[\omega t + \frac{4\pi x_o}{\lambda} \sin \omega_v t\right]$$

This signal has an FM spectrum and can be expanded into an infinite series of Bessel function sidebands:

$$\begin{aligned} i_{ac} = 2\sqrt{I_{LO} I_S} \Bigg[& J_o\left(\frac{4\pi x_o}{\lambda}\right) \cos \omega t \\ & + J_1\left(\frac{4\pi x_o}{\lambda}\right) \cos (\omega + \omega_v)t \\ & - J_1\left(\frac{4\pi x_o}{\lambda}\right) \cos (\omega - \omega_v)t \\ & + J_2\left(\frac{4\pi x_o}{\lambda}\right) \cos (\omega + 2\omega_v)t \\ & - J_2\left(\frac{4\pi x_o}{\lambda}\right) \cos (\omega - 2\omega_v)t \Bigg] \\ & + \text{higher order sidebands.} \end{aligned}$$

For large vibration amplitudes x_o, and for low vibration frequencies ω_v, the set of sidebands approaches a continuum over the range $\omega \pm \frac{4\pi x_o \omega_v}{\lambda}$.

The required frequency range over which the receiver circuit must respond is therefore $\frac{8\pi x_o \omega_v}{\lambda}$. This "bandwidth" is determined then by the vibration characteristic product $x_o\omega_v$, and of course the laser wavelength λ. It has been assumed that this product $x_o\omega_v$ is a maximum at the lowest frequency of interest (10 Hz in this case); that is, we assume that the mechanical response x_o falls off with increasing frequency at least as fast as $1/\omega_v$ across the entire range of ω_v. For the experimental surface model that has been tested, this assumption seems to be valid above the fundamental resonances of the structure. For the parameters in the breadboard design and performance calculations, we have taken $(\omega_v)_{min}/2\pi$ = 10 Hz, $(x_o)_{max}$ = 1/4 inch, and λ = 6328Å; these values imply a frequency range of 2.5 MHz peak-to-peak at the receiver front end.

For small vibrations we note that all the high order Bessel functions are small, and therefore it is sufficient to make the approximations:

$$J_o(\delta) \to 1$$

$$J_1(\delta) \to \frac{\delta}{2} \qquad \text{for small } \delta$$

$$J_n(\delta) \to 0 \quad \text{for } n>1$$

Therefore the ac current <u>for small x_o</u> becomes:

$$i_{ac} \approx 2\sqrt{I_{LO}I_S}\left[(\cos \omega t) \pm \left(\frac{2\pi x_o}{\lambda}\right) \cos (\omega \pm \omega_v)t\right]$$

The information is now carried in the two-sideband frequency components of the current, which have peak amplitudes of

$$2\sqrt{I_{LO}I_S}\left(\frac{2\pi x_o}{\lambda}\right)$$

or r.m.s. amplitudes of

$$\sqrt{2I_{LO}I_S}\left(\frac{2\pi x_o}{\lambda}\right).$$

Essentially all of the returning light is used in producing the IF carrier component at ω. The detection process must not only recover the carrier, but must distinguish the sideband currents above the system noise in an instantaneous receiver bandwidth B. Using a relatively strong local oscillator beam and a sensitive multiplier phototube detector, the main noise contribution is from shot noise in the dc current produced by the local oscillator beam. This noise is given by:

$$i_n = \sqrt{2\ e\ I_{LO}\ B} \qquad \text{(r.m.s.)}$$

where e is the electronic charge 1.6×10^{-19} coulombs.

The detection will therefore have a unit signal-to-noise ratio when the sideband current power is the same as the noise power in the circuit. Then:

$$S/N = \frac{2\ I_{LO}\ I_S}{2\ e\ I_{LO}\ B}\left(\frac{2\pi x_o}{\lambda}\right)^2 = \frac{I_S}{eB}\left(\frac{2\pi x_o}{\lambda}\right)^2$$

or $$x_o = \frac{\lambda}{2\pi}\sqrt{\frac{e\ B(S/N)}{I_S}}$$

$$(x_o)_{min} = \frac{\lambda}{2\pi}\sqrt{\frac{eB}{I_S}}\ .$$

If we further note that a square-law detector of quantum efficiency η has the characteristic:

$$I_S = \frac{\eta\ e\ P_S}{h\nu}$$

where $h\nu$ is the energy of a photon of wavelength λ and P_S is the reflected optical power incident on the detector, we arrive at a final expression for small vibration sensitivity:

$$(x_o)_{min} = \frac{\lambda}{2\pi}\sqrt{\frac{h\nu B}{\eta P_S}}$$

For $P_S = 10^{-6}$ watts and $B = 2000$ Hz, a detector with $\eta = 10^{-2}$ gives a minimum measurable vibration amplitude $(x_o)_{min} \approx 1/4\text{Å}$ or about 0.001 microinches. Even for $P_S = 10^{-10}$ watts, the value for $(x_o)_{min}$ is 0.1 microinches, so that very small motions are always resolvable provided the assumptions above are satisfied and the instantaneous receiver bandwidth is only audio.

Analysis of Heterodyne Detection of Diffusely Reflected Light

Up to this point, the signal from the moving surface has been treated as a coherent wave with undistorted phase fronts, suitable for detection by interferometric techniques. When the surface is an optically diffuse reflector these conditions may not be true. It is easily shown (see Appendix A) that for diffuse reflectors, the average or expected value of the ac heterodyne current is reduced by a factor of $(N)^{-\frac{1}{2}}$ below that obtained with a specular surface of the same reflectivity. Here N is the square of the ratio of the illuminated spot diameter, d, to the optical wavelength:

$$N \approx \left(\frac{d}{\lambda}\right)^2$$

Thus the heterodyne ac current is attenuated by the factor $\frac{\lambda}{d}$. It is clearly desirable to make d as small as possible, but diffraction limits d to values much larger than λ, since

$$(d)_{min} \approx \frac{\lambda R}{D}$$

where D is the transmitter aperture diameter and R is the distance from the transmitter to the surface. It is evident, however, that the laser beam must be focused on the diffuse surface if d is to be minimum, and that large apertures should work better than small ones because of diffraction. The breadboard heterodyne system was designed with these results in mind.

The signal obtained from a focused spot (with equal transmitting and receiving apertures) is spatially coherent because it originates over an area no larger than the resolution limit for the receiver. Therefore the original heterodyne analysis applies, but it is necessary to estimate the value for received power by accounting for the average level of light scattered away from the receiver (geometric attenuation) as well as the uneven scattering distribution due to coherent interference effects. The geometric optical signal attenuation is easily estimated if the surface is a Lambertian reflector:

$$P_R = \frac{\left(\frac{\pi D^2}{4}\right) P_o}{\pi R^2} = \left(\frac{D}{2R}\right)^2 P_o$$

Here P_R is the signal power received in the aperture of diameter D at a distance R from the focused spot. The total reflected power is P_o. In the experiments conducted during this study, the calculated value for this attenuation P_R/P_o was approximately 10^{-3}.

Interference effects cause the heterodyne current to vary about the probable value predicted above when experiments are actually performed on diffuse surfaces. Since the phases of the contributing fields from the large number of random surface irregularities in the illuminated area add up as vectors in a two-dimensional random walk phenomenon, the probability distribution for the heterodyne current approximates a Rayleigh distribution with the Lambert's law result as a most probable value. The distribution function is:

$$F(i) = 1 - e^{-\frac{1}{2}(i/I)^2} \quad , \quad 0 \leq i$$

and the probability density is:

$$f(i) = i/I^2 \; e^{-\frac{1}{2}(i/I)^2} \quad , \quad 0 \leq i$$

where I is the most probable value for the photocurrent. Using Lambert's law, this is approximately:

$$I = \sqrt{2 \; I_{LO} \; I_S} \quad \text{where} \quad I_S = \frac{\eta \; e}{h \; \nu} \; P_o \left(\frac{D}{2R}\right)^2$$

This probability density is broadly peaked, so that there is considerable probability of having heterodyne beat values substantially different from the mean. This is apparent because the mean value of i, $E(i)$ is

$$E(i) = \int_o^\infty i^2/I^2 \; e^{-\frac{1}{2}(i/I)^2} \; di = \sqrt{\frac{\pi}{2}} \; I$$

and the mean square, $E(i^2)$ is

$$E(i^2) = \int_o^\infty i^3/I^2 \; e^{-\frac{1}{2}(i/I)^2} \; di = 2I^2$$

Thus the variance $\sigma^2 = E(i^2) - [E(i)]^2 = \left(\frac{4-\pi}{2}\right) I^2$ which is roughly 25 percent of the mean square. The only requirement here is that the focused spot have an area large compared to a square wavelength (the smallest effective roughness element). This is always satisfied in practice. Note that since these quantities describe current fluctuations, the signal-to-noise or power fluctuations are even more drastic. The ratio of the variance to the mean square is a constant unaffected by the number of roughness elements within the spot; it is therefore desirable to minimize that number for the reasons given earlier. If different areas of a surface are illuminated successively, the result at each

position represents one trial of the probability law, and therefore the result obtained by averaging the currents over several positions should be near the mean. In principle, this provides a method for reducing the statistical spread in S/N values obtained in making a measurement. Experimentally, if a number of independent areas are illuminated and the results averaged during each resolution interval for the measurement, the effect should be nearly the same as if the surface were a true Lambertian reflector. Since it is the small values of heterodyne current which interrupt the measurement, such a procedure reduces the probability of obtaining currents well below the mean which may cause signal dropouts.

The technique for accomplishing this procedure in practice is very simple. One of the mirrors in the optical system is scanned at a rate well above the highest vibration frequency to be measured. Then during each portion of a vibration cycle, the returns from several nearby surface areas are measured and averaged. The scanning mirror must move the mirror over several spot diameters at rates of several thousand scans per second. The intensity and phase changes produced on the scanning beam by the surface roughness produce a broad "noise" spectrum in the receiver, but the modulation components are all at frequencies above the maximum vibration rate and can be eliminated by low pass filtering. Thus a method exists for obtaining dependable results from diffuse surfaces which would otherwise give large fluctuations. How well the technique works in practice depends on the receiver bandwidth and therefore on the optical power available, since the full spectrum of the noise-like carrier produced by scanning must be admitted into the receiver.

A simpler but less reliable procedure is to count on the fact that signals well below the mean should be rarely obtained. This amounts to moving the transmitted beam around on the surface manually until a useful signal is achieved. This approach is subject to the effects of drafts of air and large, low frequency vibrations, which cause the beam to wander slightly about the chosen spot, usually into areas which return very much less signal. Since

these wanderings are usually at slow rates, long periods of signal dropouts may occur, and any transient or acquisition problems in the receiver are aggravated.

Depth of Focus

In connection with the results for diffuse surfaces presented above, it is useful to derive an approximate value for the depth of focus over which the heterodyne receiver gives essentially full output without readjustment of the focusing optical system. This is important for detection of very large vibration amplitudes. Above it was pointed out that with the transmitted beam focused on the surface the strongest signal is obtained, since the number of independent reflector elements in the spot is then a minimum. In that case the surface lies in the pupil plane of a very small aperture (the focused spot) whose effective near field extends a short distance on either side of the surface. One criterion for the depth of focus is then the length of the near field region, which is easily estimated. If the spot size at focus is d, the extent of the near field down the axis in one direction from the surface is

$$r \approx \frac{d^2}{\lambda}$$

Taking the total length of the region in front and behind the surface as ℓ, the depth of focus, we have

$$\ell = \frac{2d^2}{\lambda}$$

For large optical systems and small working distances, which are necessary to obtain useful values of S/N, ℓ is not a large distance. Taking the working distance as R and the transceiver aperture as D, we have

$$d \approx R\left(\frac{2\lambda}{D}\right)$$

or $\ell \approx 8\lambda\left(\frac{R}{D}\right)^2$

In the present experiments, $\frac{R}{D} = 15$; thus $\ell \approx 1800\lambda = 1140$ microns or 0.045 inches. Outside this range the heterodyne signal will decrease; the exact behavior depends on the illumination cross-section and lens aberrations in a real case. In any event it is clear that very large excursions necessarily imply some change in the signal during the vibration cycle. It should be noted that the maximum velocity points during a cycle occur at the rest position. We then expect to be able to obtain the velocity extremes, even in cases where the signal is lost near the displacement extremes.

Breadboard System

At the outset of the program it was decided that the results of the experiments would be meaningful only if the breadboard model really approximated the system performance that could be expected in a useful instrument. Therefore, a considerable part of the effort on this project was devoted to the design and construction of the breadboard heterodyne system. Operation of this breadboard device for several months has certainly justified this approach, since a number of design concepts have been reduced to practice and the operating characteristics have been determined. Stability and reliability of the interferometer adjustments during the experiments were additional advantages provided by the carefully constructed breadboard.

A number of features were initially chosen as goals in the breadboard design:

(1) As much of the light as possible should be used. This implies avoidance of stray beams from an excessive number of beamsplitter mirrors in the interferometer optical system. It also means efficient utilization of the outputs from the optical frequency translator.

(2) All adjustments must be easily made and stable, so that different experiments can easily be performed.

(3) Focusing and positioning of the output beam over a wide range must be provided. These adjustments must not affect the system alignment adjustments.

(4) The aperture must be as large as practical, so that a reasonably large working distance and sensitivity to small signals can be obtained.

(5) The receiver and demodulator circuitry must provide a voltage analog of the motion on as many different types of reflecting surfaces as possible, operating with Doppler shifts over a 2.5-MHz range at audio rates between 10 Hz and 2 kHz.

The basic system diagram, developed during the first phase of this work, was shown in Figure 1. In Figure 2 we have a schematic diagram of the actual optical system developed during this program. A number of features are worth noting.

(1) Laser. A Spectra-Physics Model 119 single-frequency He-Ne laser, operating at 6328Å with approximately 100 microwatts output, was chosen as the optical source. This device is essentially free from spurious modulations which could be troublesome in this application, and the single frequency allows large path differences to exist in the interferometer with no mode beat cancellation effects.

(2) Diffraction Frequency Translator. Frequency shifting by diffraction from radio frequency acoustic waves in water was the method selected for producing the local oscillator or reference beam for the interferometer. The diffraction cell has the following advantages:

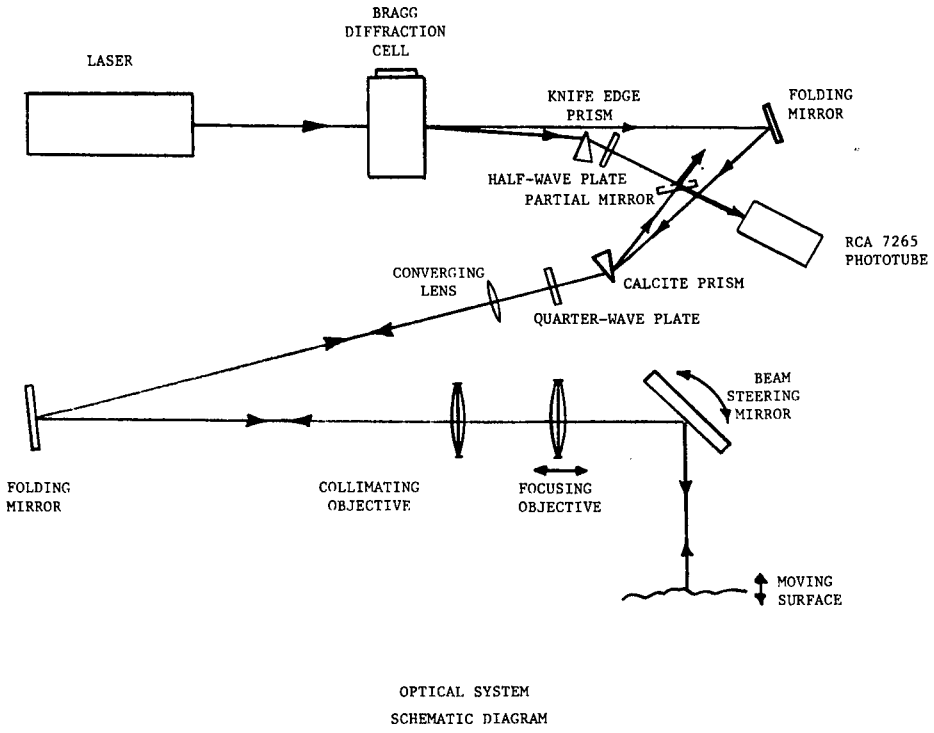

Figure 2. Schematic Diagram, Optical System.

(a) The output frequency components are cleanly separated into beams leaving the cell at different angles.

(b) The cell is reliable, relatively inexpensive to construct, does not affect the spatial coherence of the beam, and requires no adjustments in operation.

(c) The drive power required is less than one watt, and the operating frequency can be selected in the convenient range from 5 to 50 MHz. This application requires the intermediate frequency to be in this range for best results.

The frequency translator constructed for this program contains a 5-cm diameter, 5 MHz quartz transducer operating at the third overtone, 15.1 MHz. This was mounted in the end of a stainless steel tank filled with water, so that the quartz crystal was in contact with the water on one face and backed only by air on the other face. Light enters and leaves the tank through two optically flat windows on the sides. A reactive matching transformer, which efficiently couples the 15 MHz power input on the 50 ohm transmission line to the resonant crystal, is mounted in a closed metal tube attached to the tank behind the crystal. The tube eliminates radiation which would otherwise create an RFI problem in the system receiver. A similar problem exists if there is appreciable amplitude modulation on either of the beams leaving the frequency translator. This effect is always present to some extent because of scattering in the water; however, the spurious optical modulation was measured at a level of 40 db below the power in the translated beam in the present device. Methods for eliminating most of this small residual are discussed below in the section on signal detection.

Since the desired Bragg diffraction must occur for a single traveling acoustic wave only, if the diffracted light is to contain only one

frequency, it is necessary to eliminate standing acoustic waves which might interact with the light to produce spurious modulation. This can be done with an absorber in the end of the tank opposite the transducer, or by tilting that end of the tank so that the reflected acoustical wave does not interact with the light. The latter procedure was adopted here, since nothing is then introduced into the water which might contaminate the liquid and increase the scattering. This device is shown in Figure 3.

(3) Optical System. Two features of the optical system are worth noting. The first is the calcite prism and quarter-wave plate combination, which acts as an efficient optical directional coupler. The principle of operation is based on the birefringent property of the calcite prism, which has two effective angles of deviation, one for each refractive index. The light leaving the system through the prism is linearly polarized vertically; this polarization interacts only with the lower index of the calcite and is refracted through an angle along the telescope optical axis. As the light leaves the prism it passes through the quarter-wave plate, which is so oriented that the vertical linear polarization becomes circular polarization. Now light returning down the telescope axis with the same circular polarization will be converted to horizontal linear polarization by the second passage through the quarter-wave plate. Thus, received light approaches the prism polarized at 90^{o} to the plane of the transmitted light. But this is the condition required for refraction with the greater index of the crystal; thus the refracted returning signal leaves the prism along a different path from the outgoing beam. For specular surfaces at the focus of the telescope this process can be essentially 100 percent efficient -- several times better than with an additional beamsplitter mirror to do the same job. For surfaces which randomly polarize the reflected light, the efficiency drops to 50 percent, but the lost power was not suitably polarized for heterodyne detection in any case.

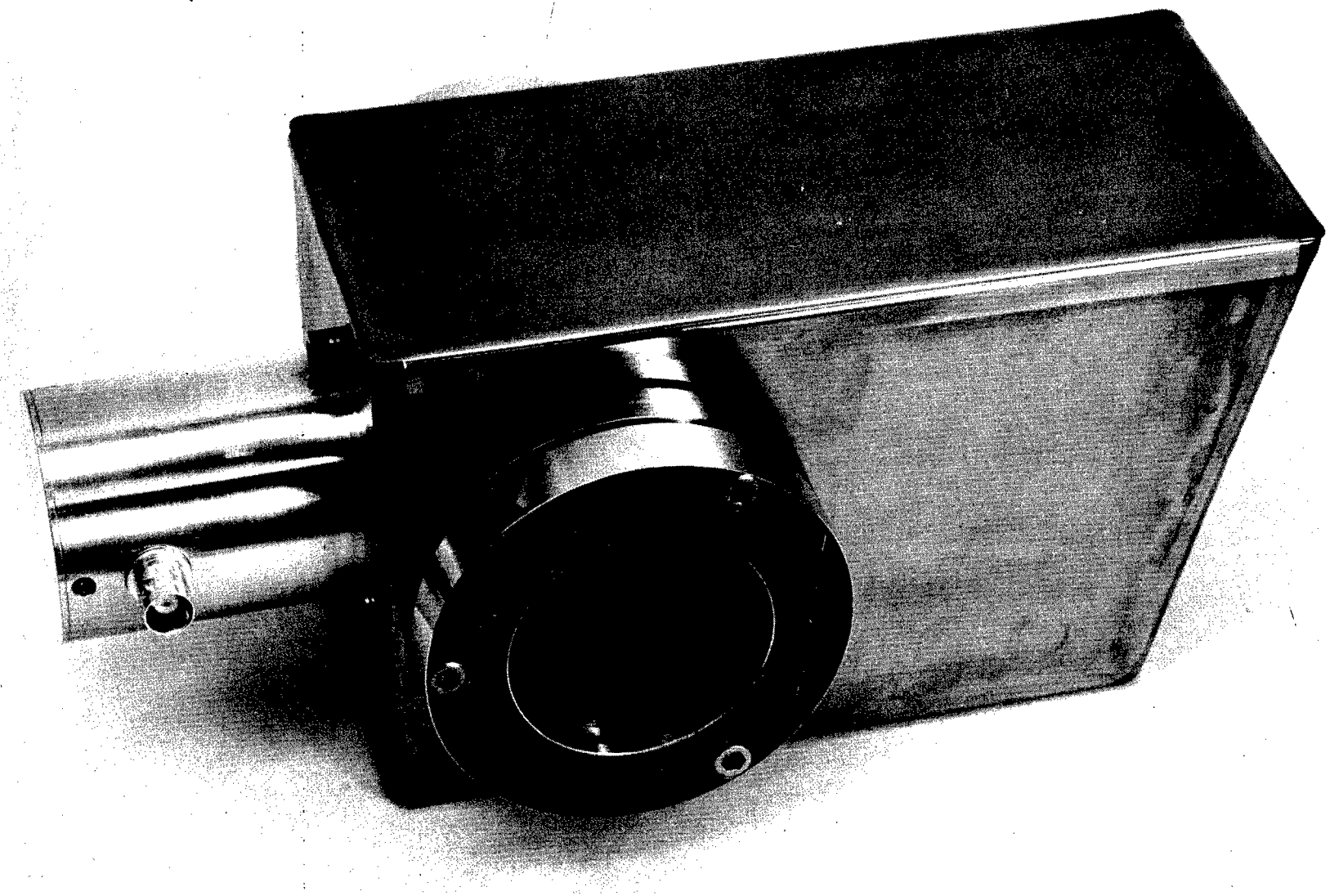

Figure 3. Diffraction Frequency Translator.

The inclusion of the optical directional coupler makes it practical to transmit and receive through the same optical system. This in turn removes the excessive mechanical alignment tolerances within the telescope optical system.which could not otherwise be avoided with heterodyne detection. These advantages occur because the moving surface is in a focal plane and reflected energy retraces its path exactly, even if some of the elements are misaligned slightly due to focusing or aiming adjustments.

A second feature of this optical system is the telescope relay system, which projects a focused spot on the vibrating surface using a pair of 3.2-inch objective lenses with focal lengths of 48 inches. The light is collimated between these lenses so that their spacing may be varied over a 10-inch range without introducing additional aberrations which might lower the heterodyne efficiency. This results in a working distance of approximately four feet that can be adjusted over a 10-inch range to accommodate three-dimensional structural surfaces. A five-inch optical flat mounted at the optical system output aperture provides a scanning capability, so that complex structural shapes can be probed using the vertical, horizontal, and depth adjustments on the breadboard.

During the tests using the beam deflector system, the beam deflector was inserted into the optical system between the directional coupler elements and the converging lens of the relay telescope, shown in Figure 2. Figures 4 and 5 show the optical and mechanical systems.

(4) Mechanical System. The optical components of the breadboard are mounted on a special three-legged metal table which Sylvania has previously used in optical systems experiments of this type. This table consists of a large machined jig-plate casting, 4 feet by 2 feet in area and 3/4-inch thick, mounted on three aluminum pipe legs 2 inches in diameter. The legs are heavily braced with side

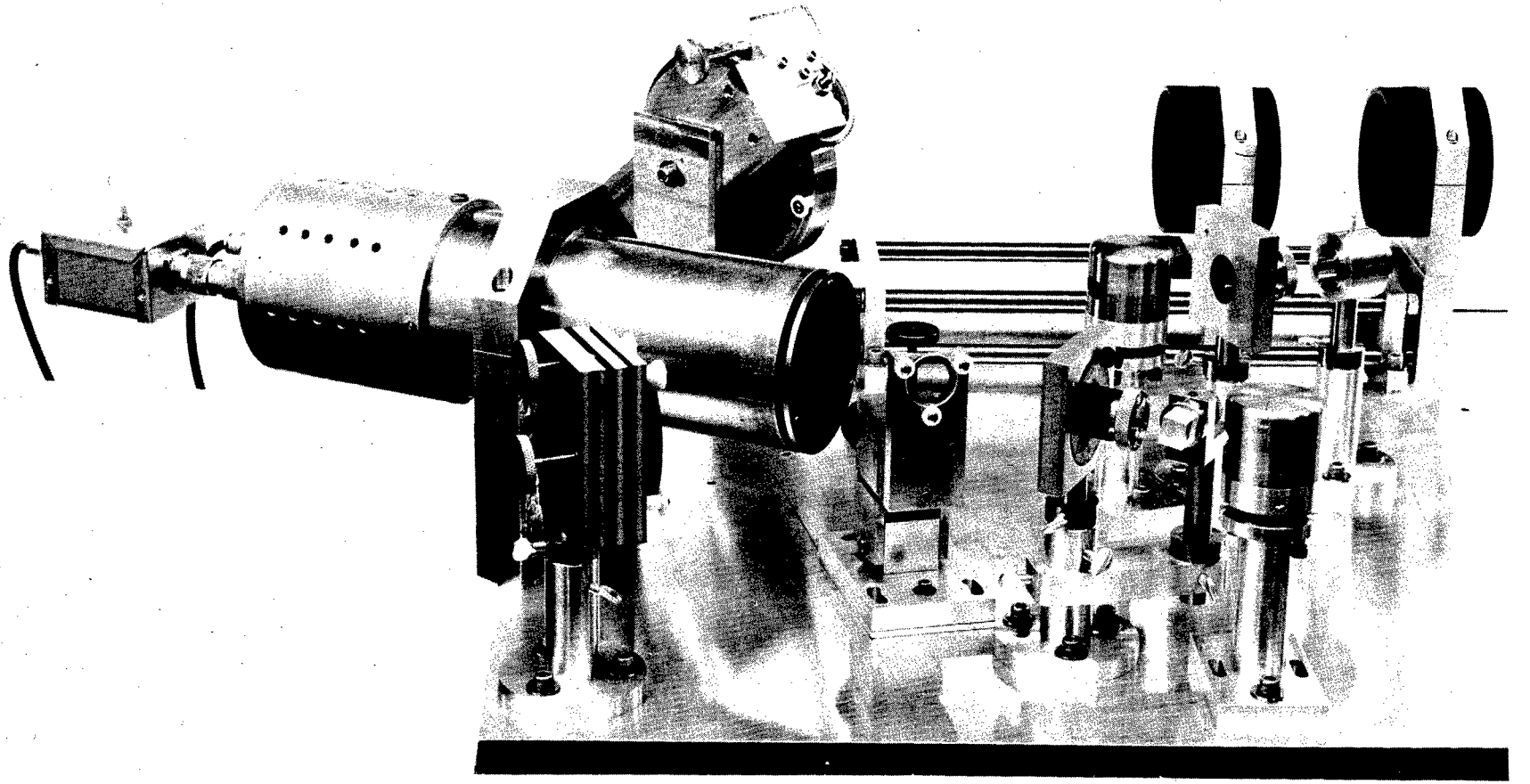

Figure 4. Photograph, Optical System.

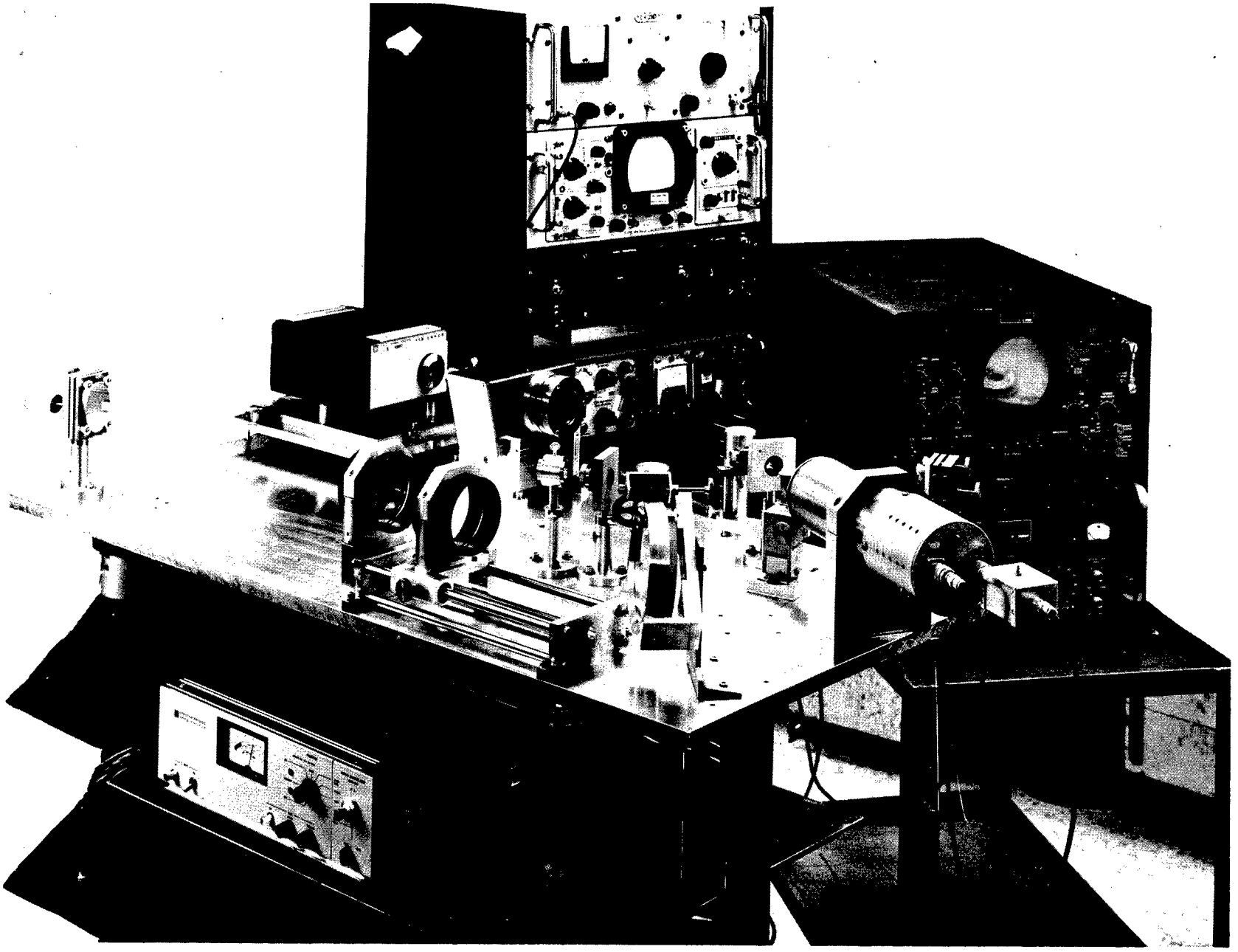

Figure 5. Photograph, Optical and Mechanical Systems.

panels, and shelves for associated electronic equipment are provided as part of the bracing. The laser and Bragg diffraction cell are mounted on fixtures which provide the necessary adjustments and can be locked in place securely. All of the precision mirror adjustments within the system are made with metal spring hinges so that no mechanical "play" is introduced. Fine adjustment of the beamsplitter alignment is made by distorting the metal block on which the mirror is supported. This approach has proved easy to use and very reliable during the course of the experiments.

No isolation of the mechanical system from floor vibrations in the laboratory environment was required in any of the tests, even though some of the vibration amplitudes measured at higher audio frequencies were as small as 1/10 wavelength. Placement of the laser power supply, which contains a cooling fan, on one of the shelves in the table structure did cause some measurable spurious modulation of the signal, but this was remedied by placing a 2-inch foam rubber pad between the power supply and the shelf.

(5) Optical Signal Detection. As shown in the optical system diagram, the present breadboard uses only a single phototube detector even though there are two beams leaving the beamsplitter mirror. This was done because only a single tube of the proper type was available in the laboratory; however, an additional 3 db of signal as well as substantial reduction of spurious amplitude modulation can be achieved when both beams are detected, as pointed out below.

The tube used in these experiments is an RCA 7265 multiplier phototube, with an S-20 photosurface and 14 stages of current multiplication. This photosurface is the best available for detection at 6328Å, with a quantum efficiency of 5% near that wavelength. A narrowband interference filter and a small aperture were mounted in front of the photocathode to eliminate the effects of room lighting.

The large number of multiplier stages can provide small signal current gains up to 20 million; however, the relatively strong local oscillator beam in this system places a much lower gain limit on the tube, since a DC current of one milliampere should not be exceeded at the anode.

In the breadboard, the voltage on the last several dynodes is reduced to limit the current to safe operating levels. The multiplier still provides considerable gain in this case, so that the noise figure of the following amplifier circuit does not have to be extremely low. It should be pointed out that the local oscillator beam produces so much photocurrent that dark noise in the tube is also negligible; in fact, the only important noise source is shot noise in the photocathode current. Ideal heterodyne detection, except for optical phase variations across the beam due to lens aberrations, is therefore easily achieved with this tube.

The advantages of detecting both beams (balanced mixer operation) were mentioned above. It is important to note that the signal modulation or beat frequency produced in detecting the beams has a 180° phase shift between the detectors, since energy is conserved at the beamsplitter mirror and no envelope variations are assumed to be present on the local oscillator and signal beams before they reach the beamsplitter. However, if power fluctuations do occur, they will produce in-phase variations at both detectors. Therefore, the ideal electrical connection to the detectors is to take the difference of their outputs, so that subtraction returns the beat signal to in-phase relationship but cancels out the power variations.

An alternative to this scheme is to use a single detector for both beams, with one beam delayed by one-half the wavelength at 15 MHz. This is a path difference of 10 meters, with the practical disadvantage that many reflections from very low-loss mirrors are required

to achieve the delay in a reasonable space. Some experiments with this technique have been carried out.

A second alternative is possible if the object is only to eliminate spurious coherent modulation at the intermediate frequency. This simply involves injection of an electrical signal of the proper phase and amplitude to cancel the undesired modulation. This is practical because the spurious modulation produced in the diffraction cell is phase coherent with the RF signal source. This fact has been confirmed experimentally, and the validity of this procedure has been verified. It has been particularly useful in making measurements of small vibration amplitudes using the spectrum analyzer, where spurious components at the carrier frequency can distort the apparent relative sizes of the modulation sidebands.

(6) Electronic Receivers.

(a) Limiter-Discriminator Receiver.- The original receiver built for this system was a straightforward design using three limiter stages and a tuned circuit discriminator. The circuit diagram is shown in Figure 6. It was found that the signal levels obtained from most of the surfaces tested were too low to produce adequate limiting in this circuit. This was because the maximum allowed DC current in the phototube anode circuit was reached before the full gain of the multiplier stages could be used. To avoid this problem, additional stages of amplification were added, until the circuit would function with test signals down to -84 dbm. The lowest measured phototube outputs were always above -70 dbm. However, shot noise across the 4 MHz bandwidth of the RF stages caused the limiters to saturate on noise when the S/N ratio referred to 4 MHz bandwidth was poor, as described below. Since the information rate is only audio, the bandwidth limit here is clearly not optimum; hence another design approach was taken.

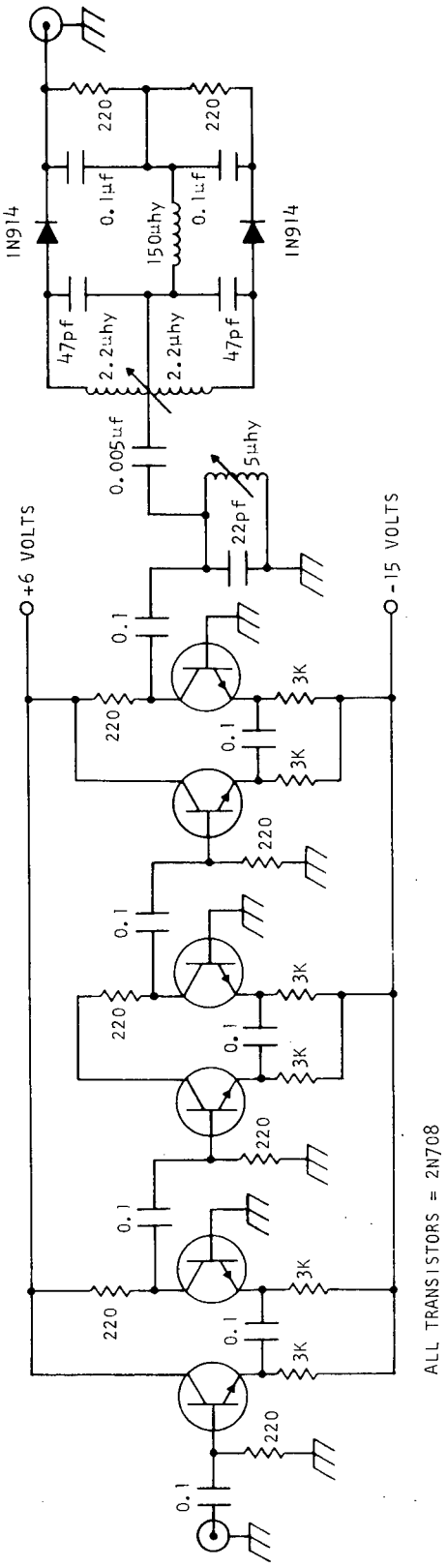

Figure 6. Schematic Diagram, Limiter-Discriminator Receiver.

(b) Tracking Receiver.- To avoid the difficulties inherent in detection of weak signals in noise with wideband nonlinear circuits, a second method was proposed and demonstrated. This new method takes advantage of the fact that the signals of interest in this applications often sweep over wide frequency ranges at low rates. Thus an ideal receiver would have a narrow instantaneous bandwidth, just adequate to accommodate the important sidebands due to the sweeping frequency, but would have a time-varying band-center frequency which follows the large frequency excursions of the signal. A practical embodiment of this concept is a heterodyne receiver circuit in which the local oscillator frequency is servo-controlled to match the incoming signal frequency exactly and maintain a constant phase relationship or zero-beat condition between the signal and the local oscillator. The voltage in the feedback loop which forces the local oscillator to track the signal frequency variations becomes the output signal of the receiver system. Such a receiver has been called a phase-locked loop.

General Characteristics:

Functionally the phase-locked loop (PLL) is a narrow-band filter that continuously servos itself to the strongest signal frequency in the input spectrum. The PLL is used to "lock-on" to the strongest incoming signal, which is shifting in frequency. The PLL utilizes active components (with gain) and a feedback loop, with the feedback loop providing the filtering and frequency servo action. The PLL is designed to accept incoming frequencies ranging from 14.0 MHz to 16.0 MHz with a passband (or noise bandwidth) of approximately 2 kHz. The PLL generally shifts the phase, making it lag by 90 degrees.

Phase-locked loops (see Figure 7) contain three main components; a phase detector, a loop filter, and a voltage-controlled oscillator (VCO). The PLL components only work together in a servo fashion when "in lock." Once out of lock, the loop behaves in a nonlinear manner.

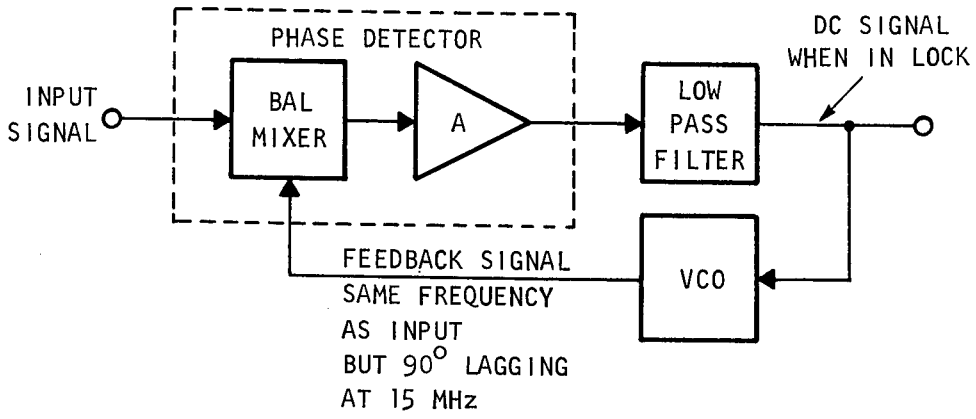

Figure 7. Block Diagram, Phase-Locked Loop.

The phase detector is a form of frequency mixing circuit in which the output is so filtered that only the frequency difference between the two input signals appears. When the PLL is in lock and the input and feedback signals are at the same frequency, the detector output is a voltage proportional to the phase difference between the signals (see Figure 8).

The output of the phase detector, as shown in Figure 8, is a DC voltage that varies with the phase difference between the input and reference (VCO) signals. As the phase difference varies from 0 to 2π, the voltage will go through the full cycle shown. For this reason, PLL systems will only stay in lock between 0 and 180° (or

180° and 360°) phase difference points. In actuality, the range is somewhat less. PLL's are usually designed to rest at the 90° phase difference points. Therefore, the feedback frequency will be 90° behind the input signal frequency. When the system is out of lock, the difference in frequency between the two signals causes the output to be a low-frequency, almost triangular-shaped wave whose frequency increases with phase difference.

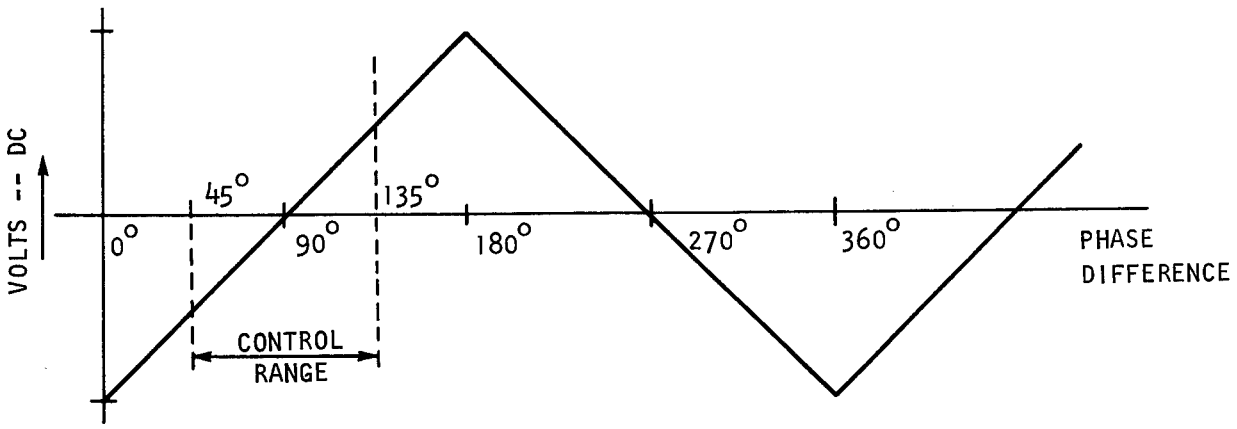

Figure 8. Phase Detector Output.

The VCO provides the feedback signal frequency. Any change in the input voltage to the VCO causes a frequency change in its output. Usually the VCO is tuned so that it normally oscillates at the center of the input signal frequency range and is biased to the higher and lower frequency extremes by positive and negative swings of the control voltage.

The loop filter sets the bandpass of the PLL and is a simple RC circuit, as shown in Figure 9. The loop filter components were calculated for a zero to 2 kHz low-pass range and the values optimized on an empirical basis.

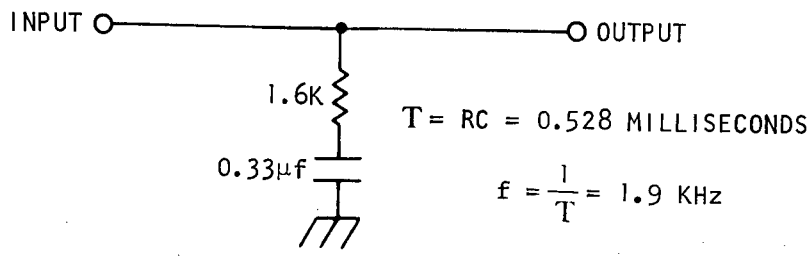

Figure 9. Low Pass Loop Filter.

Operation of Complete Loop In and Out of Lock:

The conditions for the loop being in lock are, of course, that the incoming and feedback signals are identical in frequency (though they will differ in phase). Under these conditions, the phase detector output will be a DC voltage, proportional to the difference in phase. Because of the nature of the VCO and the phase detector, there will always be varying amounts of phase difference between the input and reference signals as the system tracks the input signal over its range. The VCO needs varying amounts of voltage to change its frequency, and the phase detector can only supply these voltages at the expense of phase difference.

As shown in Figure 8, the phase difference that would occur in the system as it tracks the input signal might vary from 45 to 135 degrees. The system gains are set so that the phase detector provides control voltages large enough to cause the VCO to decrease or increase, in frequency, as the phase difference varies 45 degrees below and above the 90 degree resting phase lag.

A "safe" phase difference variation of 45 - 135 degrees has been chosen; while large ranges, say, 10 - 170 degrees, might use more of the phase detector's capability, this would increase the danger that the system would then go out of lock at 180^{o}. It stands to reason, therefore, that the smaller the phase error (ϕ_e), the more efficient the PLL will be as a filter. But, then, more gain is required in the system.

As long as the changes of input signal frequency are slow enough so that they remain within the bandwidth of the loop, and this is determined mainly by the filter, the PLL will stay in lock. However, once the frequency of the phase difference signal goes past the filter's roll-off frequency, the correction signal reaching the VCO will become so attenuated that the VCO will revert to the midpoint frequency and the system will break out of lock. Once a rapid change in the input signal has caused the loop to break out of lock, the difference between input and output signals will cause the phase detector to put out its triangular wave signal.

The higher the frequency difference between input signal and the VCO, the more the filter attenuates the signal being passed to the VCO. However, the filter time constant will allow some of the higher frequencies (although attenuated) to get through to the VCO. The VCO will sense this attenuated higher frequency signal and produce corresponding fluctuations around its resting frequency. These will build up around the loop, and eventually provide a reference signal at a frequency that coincides with the input signal frequency and at the point lock will occur.

There is a trade-off between the narrowness of the PLL bandpass, the speed with which the PLL can respond to input changes, and the ease with which the PLL can re-acquire lock. The narrower the filter bandpass, the narrower the bandpass action of the overall PLL. On the other hand, a narrow bandpass means that the PLL is more likely to come out of lock. A "lock-on" aid could be incorporated by switching in a filter with a wider bandpass until lock is re-acquired and then switching back to the narrow bandpass filter.

PLL Design Parameters:

(1) Tracking range (minimum) - 14.0 MHz to 16.0 MHz.

(2) Loop bandwidth $\approx$ 2 kHz.

(3) Permissible phase error (ϕ_e) - 90^o (45^o on either side of center).

(4) Gain - balance mixer $\approx$ 0.4 V/radian (assumed).

(5) Required loop gain - $G = \frac{\Delta f}{\sin \phi_e} = \frac{2 \text{ MHz}}{\sin 90^o} = 2 \times 10^6$.

(6) Gain of VCO 1 MHz/volt.

(7) Gain of VCO and phase detector -

$$G' = (G_{VCO})\ (G_{\phi\ DET}) = \frac{(1 \times 10^6 \text{ cps/volt})\ (0.4 \text{ volts/radian})}{2\pi}$$

$$G' = 0.636 \times 10^6.$$

(8) Gain to be added to loop by amplifier -

$$G_{amp} = \frac{2 \times 10^6}{.0636 \times 10^6} = 31.4.$$

The mixer being used is an HP Model 10514A, a balanced mixer which will operate between 0.2 MHz and 500 MHz and is designed for use with 50-ohm systems. The amplifier stage is a single-ended non-inverting DC amplifier which uses a Fairchild μa 702 operational amplifier for its active element. The voltage gain of the amplifier is approximately 32 which is required to provide the necessary total loop gain. See Figure 10 for complete schematic of the PLL system.

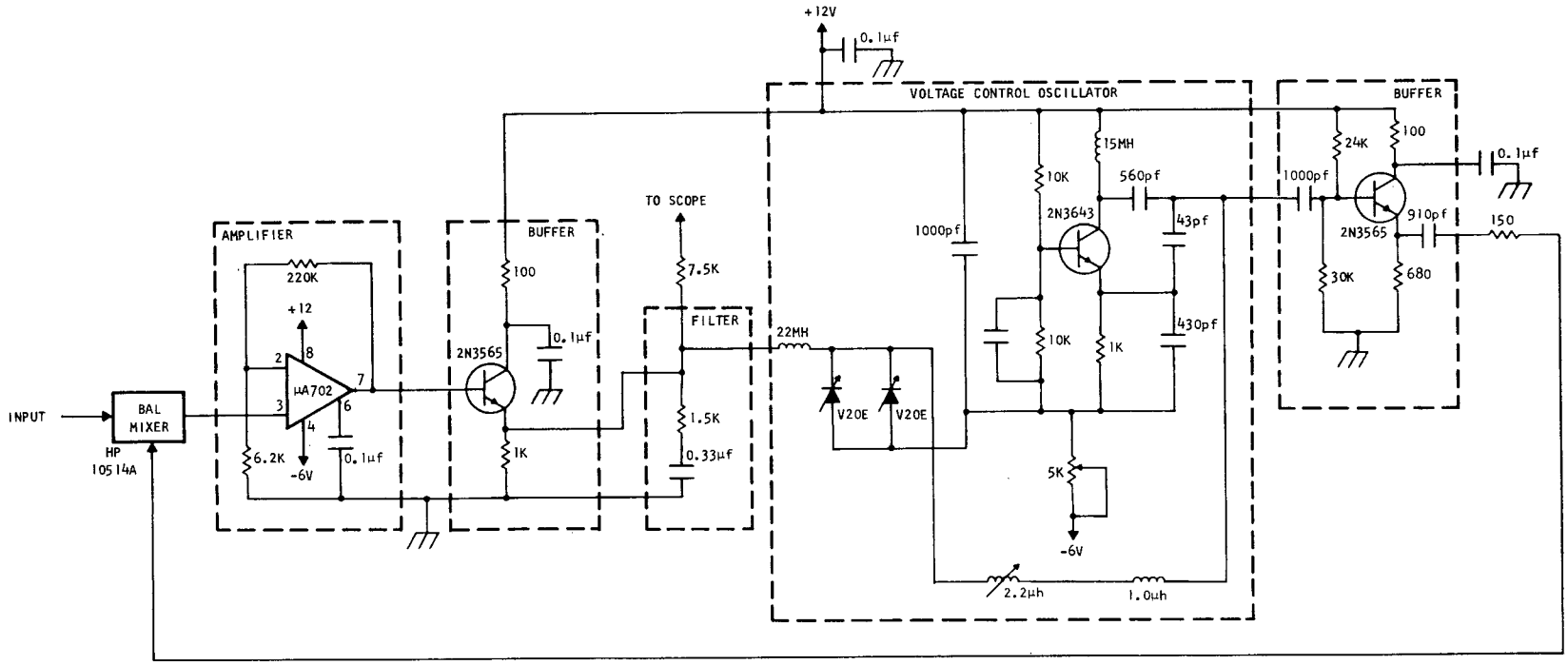

Figure 10. Schematic Diagram, Tracking Receiver.

Experimental Results

Spectrum Analyzer Tests.- Tests of the optical breadboard were initially performed using the radio-frequency panoramic spectrum analyzer as the receiver. Alignment of the optical system using an external specular surface was accomplished in this way. By substituting calibrated signals of known power for the actual signal obtained from the multiplier phototube, it was possible to measure the relative signal strengths obtained with the system operating on various surface materials. Typical values for signal levels are listed in the following table.

Reflecting Surface	Heterodyne Signal Output
Aluminized Mirror (specular reference)	-15 dbm
White Scotchlite tape	-25 to -60 dbm
White paper	-47 to -60 dbm
Flat white paint	-50 to -60 dbm
Aluminum paint	-35 to -55 dbm
Residual AM on reference beam	-55 dbm
Noise (Δf = 2 kHz)	-75 dbm.

The fluctuations indicated in the levels for non-specular surfaces reveal the usual interference effects due to random diffraction-lobe location with respect to the system receiving aperture. The values listed were the frequently observed limits of the signal variations during many seconds of observation time. Power fluctuation rates depend on mechanical stability in the beam position at the surface and thermal stability of the atmosphere over the short path from the instrument to the surface. Typical rates are below a few cycles per second. Since the spot size on the surface is less than 0.1 millimeters in diameter, very small effects can cause large amplitude variations.

The heterodyne mixing efficiency was estimated by measuring the optical signal powers and losses at various points in the optical system, and then

comparing the calculated phototube signal-to-noise ratio to that obtained in practice. The value thus obtained was approximately 10%, although measurements made later with the system readjusted indicated possibly twice this efficiency. This quantity measures the effect of aberrations and misalignment on the heterodyne beat signal; it is unity for an aberration-free system. It is of interest that less than 50% of the laser power was incident on the surface, due primarily to lens reflection losses in the breadboard optical system. With every refractive element coated for minimum reflection and very low loss mirrors, essentially all of this loss can be eliminated. This indicates that a well-engineered working instrument can have performance substantially better than this initial breadboard version.

When the surface was vibrated, the velocity spectrum could easily be examined using the spectrum analyzer. With the analyzer scan rate properly set, the effects of amplitude fluctuations on this display usually are not objectionable, since some time-averaging is performed.

Spectra of this type, obtained by driving the electrodynamic shaker attached to the surface model, are shown in Figure 11. At the lower frequencies the motion amplitude is many wavelengths; thus the sidebands are unresolved but the spectral spread is considerable, as in Figure 11 (a) and (b).

At higher frequencies the sidebands are fewer and spaced so that they are resolved, as in Figure 11 (d) and (e). Since the vibration frequency is known, the amplitude can be determined from the spectrum, either from the overall spread (indicating the peak-to-peak Doppler shift) at low frequencies and large amplitudes, or from a table of Bessel functions for small vibrations at frequencies for which the sidebands are resolved.

As an example, consider again the spectrum of Figure 11 (a). The sideband spread, measured by the calibrated marker in the spectrum analyzer, is 100 kHz.

Figure 5. **Photograph, Optical and Mechanical Systems.**

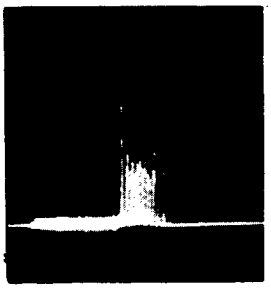

(a) 100 Hz
Doppler Spread ~100 kHz

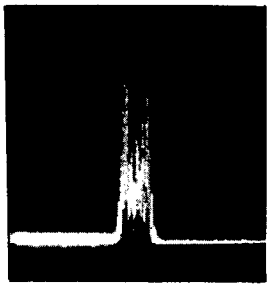

(b) 1000 Hz
Spread ~50 kHz

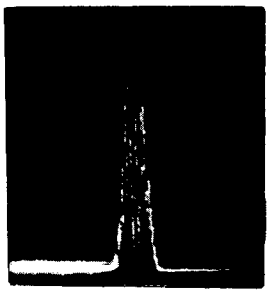

(c) 2000 Hz
Spread ~50 kHz

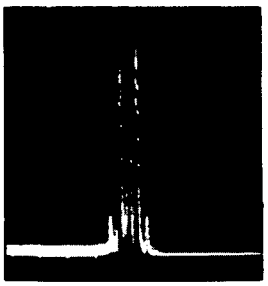

(d) 5000 Hz
Spread ~10 kHz

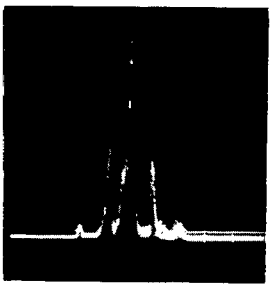

(e) 5000 Hz
(analyzer scale expanded)

Figure 11.

Spectra obtained from model surface with aluminum paint at various vibration frequencies.

Half of this spread is:

$$\Delta f = \frac{2x_o \omega_v}{\lambda} = \frac{4\pi x_o f_v}{\lambda}$$

using a result derived earlier in the analysis above. Therefore, the peak-to-peak motion amplitude is

$$2x_o = \frac{\lambda \Delta f}{4\pi f_v} \times 2$$

In this case, $\Delta f = 5 \times 10^4$ Hz, $f_v = 100$ Hz, $\lambda = 6.33 \times 10^{-4}$ millimeters. Thus

$$2x_o = \frac{6.33 \times 5x2}{12.56 \times 10^2} = 5.0 \times 10^{-2} \text{ mm} = 50 \text{ microns.}$$

As a second example, take the spectrum of Figure 11 (e). Here the first sidebands, corresponding to first order Bessel functions, are about half the amplitude of the carrier, corresponding to the zero order Bessel function. From a table of these functions, the first solution for δ in the equation:

$$\frac{J_1(\delta)}{J_o(\delta)} = \frac{1}{2}$$

is for $\delta \approx 0.9$. Since $\delta = \frac{4\pi x_o}{\lambda}$, this implies that $2x_o$ is $\frac{0.9}{2\pi}\lambda$, or 0.09 microns. The fact that such a small amplitude is easily measured, even for surfaces such as the aluminum paint in this case, indicates the usefulness of the heterodyne technique.

Surface motions up to 6 mm peak-to-peak were also measured using small surface samples mounted on a modified loudspeaker voice coil adapted for this purpose.

Modes on the structural surface model were also observed with the spectrum analyzer receiver. This was done by moving the beam over the surface using the 5-inch steering mirror and measuring the spectrum width at each point by the methods just outlined in the examples above. A typical scan is depicted in Figure 12, taken on an aluminum-painted area on the structural surface model. The spatial standing wave pattern set up by a vibrational resonance at 300 Hz is indicated by the widths of the spectra at positions (a) through (e). This 4-inch scan covers approximately one-half of a spatial period of the mode, with a normal velocity maximum located at the center of the scan.

A correlation between data taken in this manner and data taken using the interference mapping technique is described in the experimental section of this report for the interference technique.

Limiter-Discriminator Tests.- As soon as the limiter-discriminator circuit was completed, it was tested in conjunction with the optical system and the various simulator target surfaces. On the specular surfaces, the circuit demodulated the target velocity information very well. With Scotchlite reflective tape as a surface, the demodulated signal was often very good, but there were frequent dropouts when the optical signal faded due to interference. At first no signal could be obtained from the other diffusely reflecting materials. At this point, gain was added to the receiver and a new plasma tube was put in the laser. The results of Figure 13 are indicative of the better performance obtained with these changes. Again the specular surface gave very good results, with useful results from Scotchlite tape and poor results on white paper.

The poor performance on "flat" diffuse reflectors is caused by a characteristic of FM receivers of this type. This circuit must accommodate modulations of the 15 MHz carrier at very high deviation ratios, sometimes as great as 10^3 to 10^5. Thus the information bandwidth is quite small, only 2 kHz, but the front end bandwidth in the RF stages must be at least 2.5 MHz. Provided the limiting occurs due to signal voltage variations in the IF strip, the

Position: (a) 2 inches left

(b) 1 inch left

(c) Center

(d) 1 inch right

(e) 2 inches right

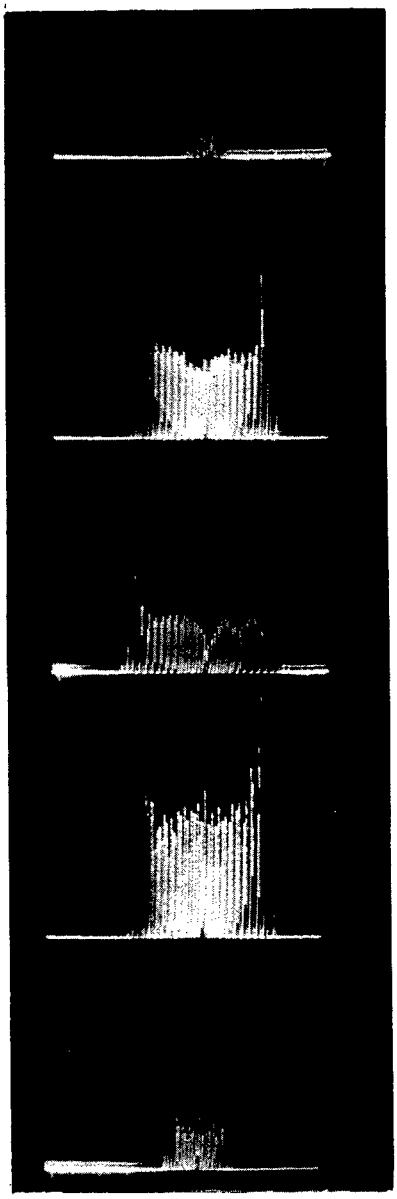

Figure 12.

Vibrational mode pattern spectra from aluminum painted surface. Samples taken at intervals around model circumference. Resonant frequency 300 Hz. Width of spectrum indicates relative amplitude.

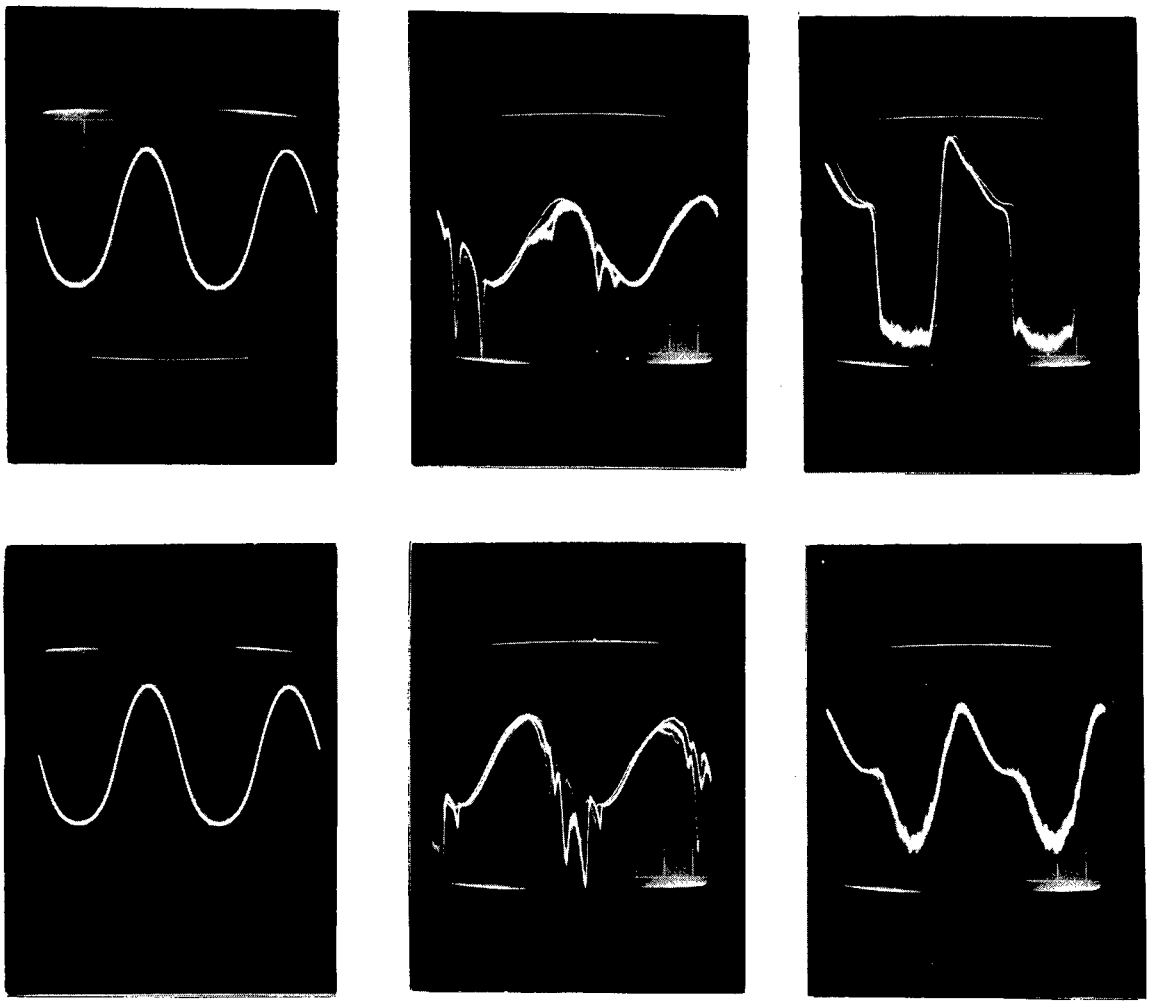

(a) Aluminized Mirror (b) Scotchlite Tape (c) White Paper

Figure 13.

Limiter discriminator output.
Vibration double amplitude = 1 mm,
frequency = 100 Hz.

Output voltage is proportional to
surface velocity.

narrowband filtering in the post-detection audio stages is effective, and receiver performance is good. The signal-to-noise ratio is that obtained for a 2 kHz bandwidth. However, if the modulated signal falls below the rms level of shot noise, referred to the front end bandwidth, the limiting is no longer on signal but on broadband noise. The IF amplifier is then saturated at times which have no relation to periods of maximum signal voltage, and the post-detection filtering is not effective. The receiver behaves as though the information bandwidth had expanded to greater than 2.5 MHz. For this reason, the circuit fails to provide optimum response for weak signals.

Tracking Receiver Tests.- The tracking receiver was designed to avoid the weak-signal limitations of the previous approach. A description of the theory of operation of this receiver, as well as the design parameters, was given above in the discussion of the experimental breadboard circuitry.

Preliminary tests of the first tracking circuit, with a servo bandwidth of only a few hundred cycles per second, indicated that the small-signal performance was greatly improved over the original limiter-discriminator design; however, there was some problem in acquisition of the "lock-on" condition when the signal was interrupted. Widening of the filter characteristic to approximately 2 kHz eliminated the signal acquisition difficulties, apparently because large phase shifts occur only at rates low enough for good tracking with this bandwidth. It is interesting to note that the servo loop bandwidth may be less than the information bandwidth, since tracking is only required to keep the mixing RF signals near phase quadrature. The mixer acts as a phase demodulator even for frequencies at which the servo loop gain is greatly reduced. In other words, error signals can exist at some points in the circuit even though the control loop fails to respond to these signals. System bandwidth would then be determined by the bandwidth of the audio circuitry which processes the error signal output.

Results obtained with the modified tracking receiver were generally acceptable on all surfaces, with occasional signal dropouts on the white

paper, white paint, and reflective tape surfaces. The flat white paint appeared to give the worst performance, while aluminum paint was nearly as good as the reflective tape for near-normal incidence.

Figure 14 shows typical large vibration amplitude waveforms obtained from a variety of surface samples attached to the vibrating loudspeaker coil. The frequency spread here was 2.5 MHz. Results at small amplitudes were also excellent; frequency shifts of the order of 1000 Hz were easily measured, with the limit at that level set by residual RF leakage and hum pickup in the breadboard circuit, rather than by shot noise. For the aluminized mirror surface, sensitivity was sufficient that tracking could be obtained at any position of the focusing objective within its range of several inches.

The performance of the circuit at very low optical signal levels is indicated in Figure 15. In this test the optical signal was deliberately attenuated to levels near the receiver threshold. As the output voltage traces indicate, the voltage controlled oscillator returns to its free-running (zero signal) condition more frequently as the signal amplitude diminishes. However, the portion of the cycle over which tracking does occur remains a reasonably good record of the surface velocity at that time.

Using this receiver, tests were made of the beam dither technique described earlier in the section on heterodyne detection of diffusely reflected light. The output beam was scanned sinusoidally over the vibrating surface at a 2 kHz dither frequency, using a mirror on a resonant suspension driven by an electrodynamic coil. Dither amplitudes of several spot diameters were easily achieved in this way.

The effect of beam dither on the receiver output waveform is shown in Figure 16. The surface vibration frequency in this case was approximately 200 Hz, with a vibration level providing a peak frequency shift of 0.5 MHz. The frequency modulation due to the 2 kHz scan appears as an additive modulation. As the scan amplitude is increased, the receiver begins to drop out

Material: (a) Aluminized Mirror

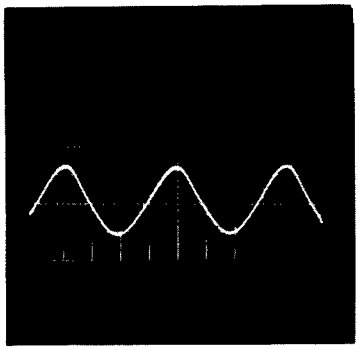

(b) Scotchlite

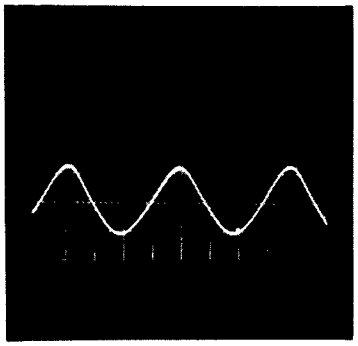

(c) Flat White Paint

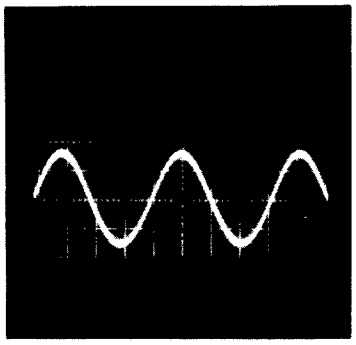

(d) Aluminum Paint

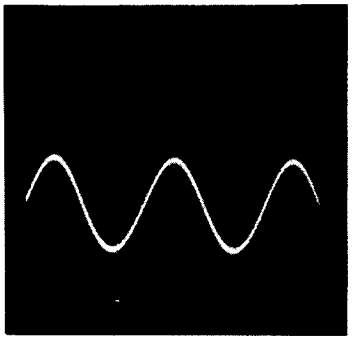

Figure 14.

Tracking receiver output with various surface materials. Vibration double amplitude ≈ 1 mm, frequency ≈ 100 Hz. Output voltage is proportional to surface velocity.

(a)

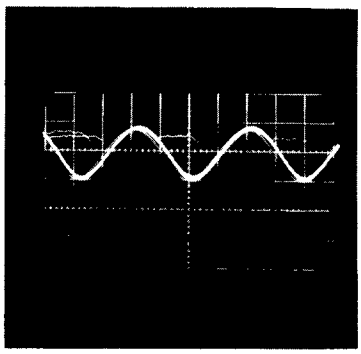

(b)

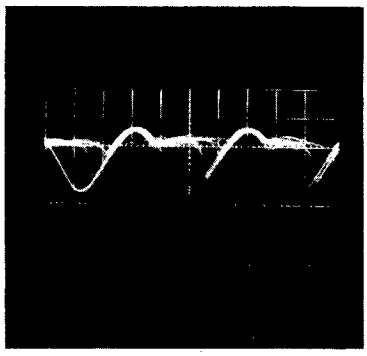

(c)

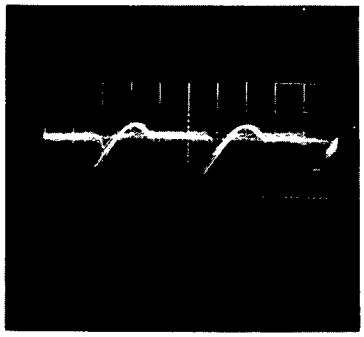

(d)

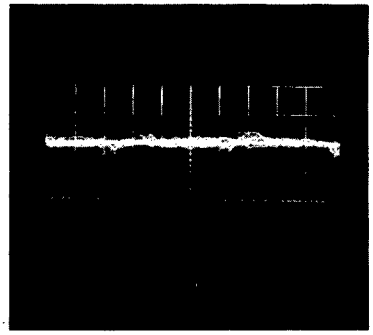

Figure 15.

Tracking receiver output near sensitivity threshold. Optical signal level decreasing from (a) through (d).

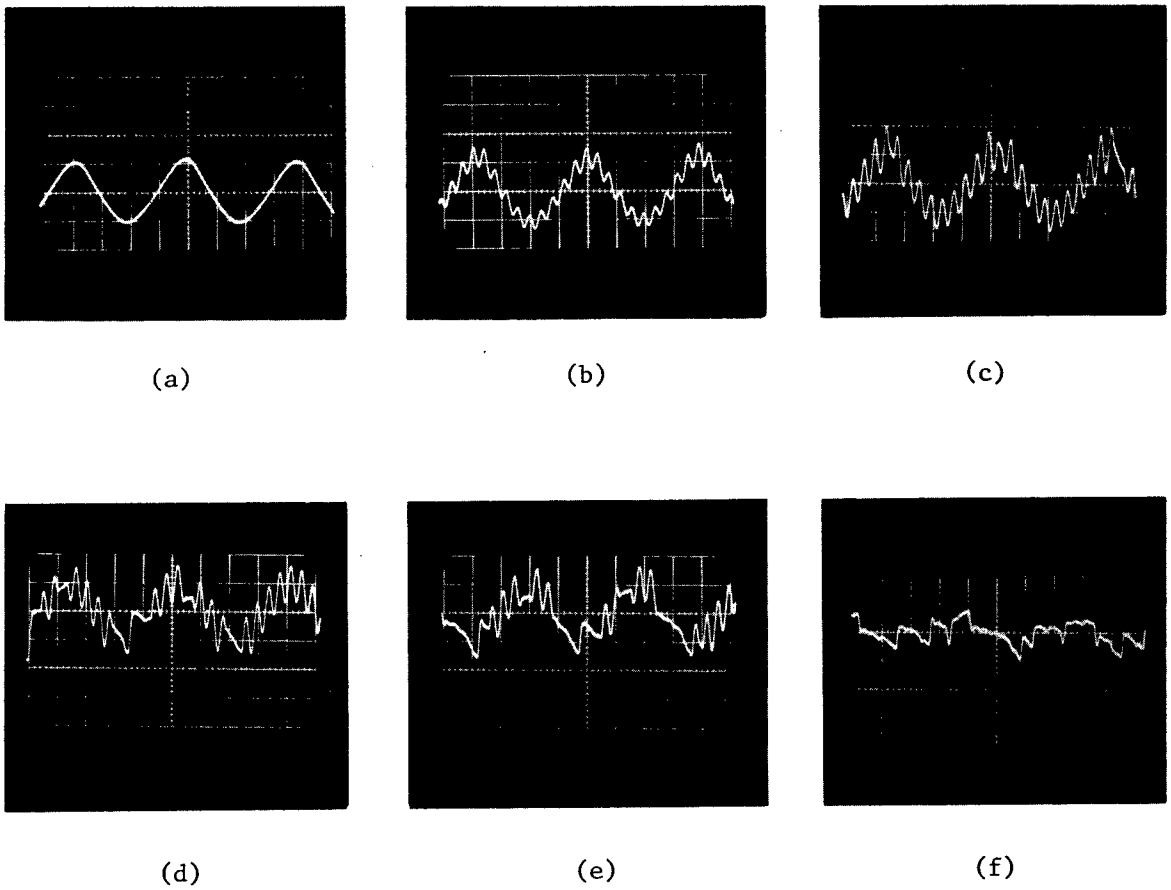

Figure 16.

Effect of beam dither amplitude on tracking receiver output. Dither frequency = 2 kHz, peak Doppler shift ≃ 0.5 MHz. Dither amplitude increasing from (a) through (f).

of lock more frequently. At amplitudes of only three spot diameters, the output was often similar to that of Figure 16 (f), which bears little resemblance to the original signal. Thus the tracking fails just at levels where statistical averaging becomes useful.

The problem here seems to be the roughness of the surface. Motion of only one spot diameter apparently provides so large a phase shift that the receiver cannot follow the frequency variations. The scan rate must be above the vibration frequency in order for cycle-to-cycle averaging to be achieved. Thus the sidebands from the dither can easily extend beyond the frequency range over which the receiver is designed to work. The broad extent of the dither-induced sidebands was verified using the spectrum analyzer to display the heterodyne signal, as in Figure 17. The variations in the spectral envelope caused by focusing adjustments were clearly revealed. This spectrum, of course, contains both amplitude and frequency modulation sidebands, since both effects are present in the composite signal from the many randomly-phased surface elements illuminated periodically by the sweeping beam.

It may still be possible to achieve signal enhancements using the dither method, perhaps with a slower scan rate combined with a synchronizing technique in which the output display is triggered only when the beam arrives at a point on the surface providing sufficient optical power to allow the receiver to track. Some further investigation beyond the results of the present study may be justified, therefore.

Additional Experimental Data.- The focal depth calculation made earlier was checked using the aluminized mirror as a reference surface. This mirror was mounted on a micropositioner so that it could be moved along the axis of the transmitted beam near the focal region. The heterodyne signal was measured by substitution at each point along the axis. The following table gives the signal relative to that obtained at the best position, versus distance away from the optimum spot.

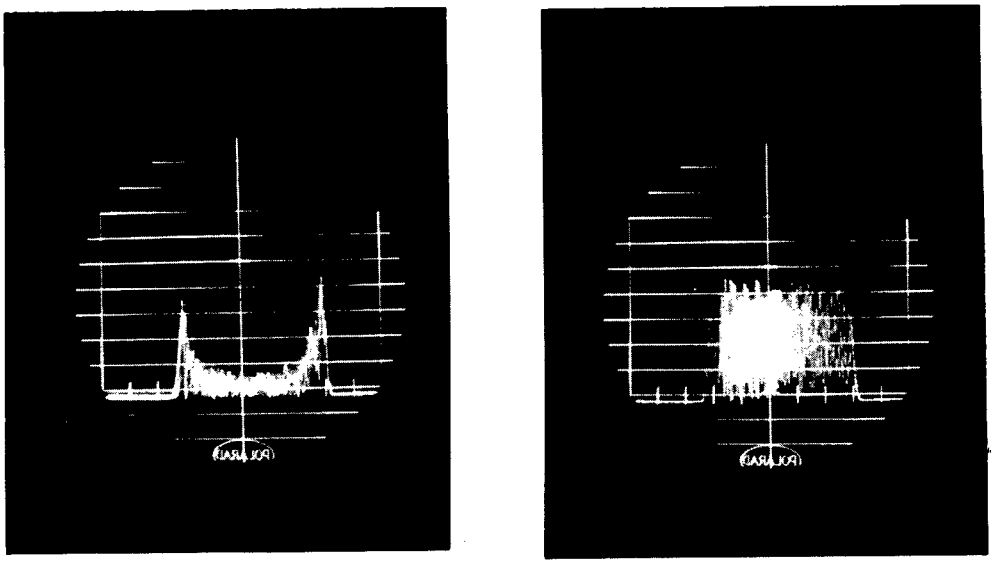

Figure 17.

Spectra obtained with 2 kHz beam deflector. Dither ~ 3 spot diameters. Two slightly different focal adjustments. Spectral spread ~0.5 MHz.

Distance From Maximum (Inches)	Relative Signal (db) Toward Receiver	Away From Receiver
0.000	0	0
0.025	-3	-3
0.050	-8	-7
0.075	-12	-11
0.100	-15	-14
0.125	-17	-16
0.150	-18	-17
0.175	-19	-18
0.200	<-20	-20
0.225	---	<-20

From this experiment, the "3 db zone" for specular reflectors is slightly greater than one millimeter in length. Although consistent measurements could not be made on diffuse reflectors because of the fluctuations, it is reasonable to expect the zone to be roughly twice as long. This should be true because the diffuse surface destroys the phase coherence and acts as a source located in the plane of the surface. However, the specular mirror forms a virtual image of the focus which is located twice as far from the original focus as the mirror surface.

Tests of methods for reducing the effects of the spurious 15 MHz amplitude modulation on the reference beam were also conducted. One approach was to delay one of the optical beams leaving the beamsplitter mirror by a time equal to one-half period at 15 MHz and then return this light to the phototube along with the other direct beam. This makes the heterodyne modulation add in phase and the amplitude modulation add out of phase. The delay was accomplished using two multilayer dielectric mirrors spaced one meter apart. Multiple reflections provided the necessary ten-meter path difference. The mirrors were attached to the breadboard using temporary optical bench clamps. Results indicated some reduction of AM could be achieved in this way, but attenuation was required in the direct beam to make the modulations cancel. This attenuation reduced the heterodyne signal; for this reason further experiments with this method were not carried out.

A second, very successful technique was then demonstrated. This involves the addition of a suitably phased RF signal to the heterodyne output, so that the residual AM signal is cancelled. This was done by taking power from the signal source for the diffraction cell. The injected signal was passed through a large isolation resistor and added to the signal leaving the multiplier phototube. A variable attenuator and coaxial delay line were used to adjust the phase and amplitude for best suppression of the spurious 15 MHz modulation. It was found that the best adjustments reduced the undesired signal to an unmeasurable level, using the spectrum analyzer or the other receivers. This experiment proved that even without balanced mixer operation, a single detector can be used with no AM interference from the frequency translator.

Of course, these methods are of interest only in experiments in which only a single optical detector can be used. In an operational instrument, the balanced mixer configuration with two detectors is always superior.

INTERFERENCE MAPPING

The interference mapping technique is a method, developed during the initial study phase of this work, for obtaining qualitative information about the vibrational modes of diffuse reflectors. It is of practical interest because it can greatly reduce the number of surface points at which quantitative data is needed, and easily presents a graphic picture of the surface motion even for very complex modes. During this phase of the study, the technique was investigated experimentally using the cylindrical model structure excited by the Goodmans shaker. Comparisons of results obtained in this way with scans made using the heterodyne system were made. Also, the effects of different surface paints on the visibility of the interference patterns have been noted. The method has also been extended to include precision measurement of the axis of rotation of diffusely reflecting objects.

Analysis

The basic configuration used in interference mapping is shown in Figure 18. A large area on the object is illuminated by the laser beam, and the interference produced by the diffusely reflected light is viewed in some plane in front of the surface using a lens and iris diaphragm. From simple ray optical considerations, it is clear that the iris permits only a small area on the surface to reflect light through a point in the interference plane and <u>also</u> through the iris. The fraction of reflected light that satisfies this geometrical condition is useful for viewing the pattern. Note that there is good correlation between points on the surface and points in the observed pattern. The approximate width of a surface region within which all points reflect useful light through a single point in the observed pattern is given by:

$$\omega_r = \omega_i \frac{L_r}{L_i} ,$$

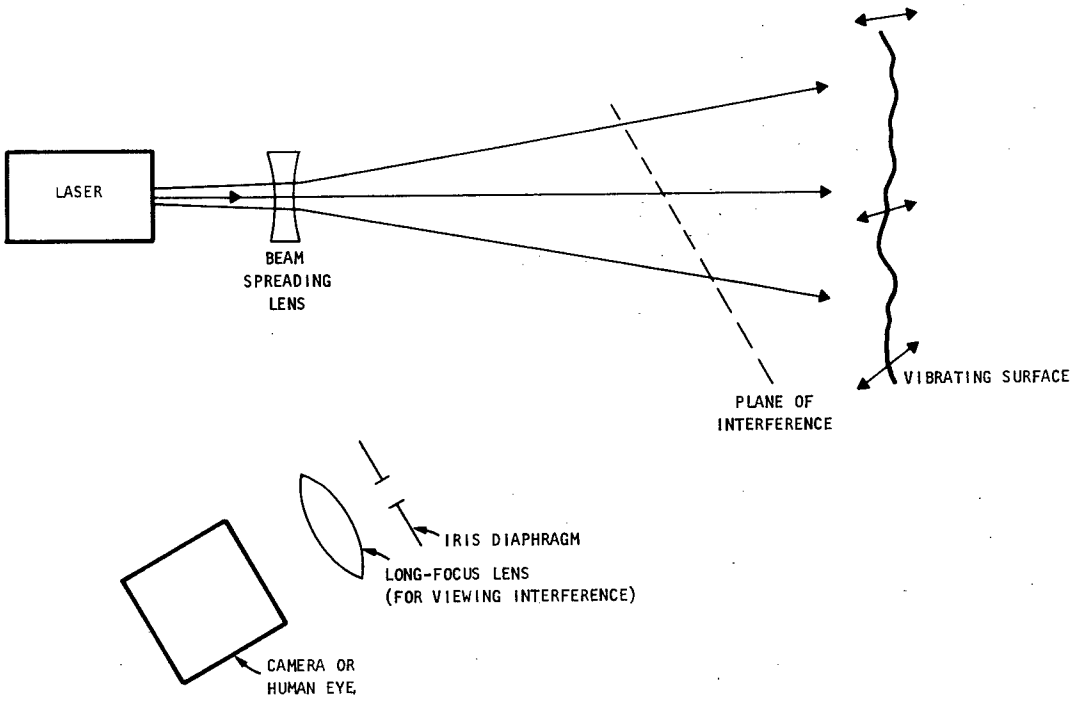

Figure 18. Interference Displacement Mapping System.

where ω_r is the diameter of the region, ω_i is the diameter of the iris, L_r is the distance between the region and the interference plane, and L_i is the distance from the plane to the iris. For normal viewing the focal length of the viewing lens is made equal to L_i.

The sensitivity of the method depends on the fact that the width ω_L of a lobe (a bright spot) in the interference pattern is given by:

$$\omega_L = L_r \frac{\lambda}{\omega_r} = L_i \frac{\lambda}{\omega_i} .$$

Since this is a diffraction-limited interference effect, a uniform change in phase across ω_r of about one cycle will move the lobe laterally through a distance roughly equal to its width. A tilt of the surface due to a gradient in the normal component of displacement will accomplish just such a phase shift if the differential displacement is about $\lambda/2$ across the distance ω_r. For differential displacements greater than this, at frequencies unresolved by the human observer or the photographic exposure, the pattern areas corresponding to the tilting surface areas will be streaked in the direction of the gradient. This streaking of the interference pattern is the effect of interest using this method. The vibration level at which streaking begins to appear is therefore that amplitude for which the peak difference in displacement for points on the surface separated by ω_r is just $\lambda/2$. The minimum tilt angle is therefore:

$$\alpha = \frac{\lambda}{2\omega_r} = \frac{L_i}{L_r} \frac{\lambda}{2\omega_i} .$$

Thus if the motion is to be resolved over surface elements as small as 5 millimeters ($=\omega_r$) and the wavelength is roughly 10^{-3} millimeters, the minimum detectable tilt angle is 10^{-4} radian, and the peak differential displacement is of course 10^{-3} millimeters. Sensitivity in this range is useful because it is good enough for many practical applications yet not so good that minor ambient vibrations disturb the result.

The effect of translation of the surface during observation is of importance for applications in which the structure is excited by a linear displacement, as in a shake table test. The interference is directly correlated with the position of the surface if the illuminator is located at any practical distance from the structure. Therefore a translation of the structure through a distance Δx imposes an identical displacement in the pattern. Since Δx will always be present at some level, it is important to determine how large it can be before it substantially affects the sensitivity of the method. This is easily found by equating the translation and the lobe width:

$$(\Delta x)_{max} = \omega_L = L_r \frac{\lambda}{\omega_r} = L_i \frac{\lambda}{\omega_i} .$$

In a real situation, λ and Δx may be fixed. But L_i and ω_i are controlled by the operator; thus if space permits, it is always possible to increase the iris distance L_i until Δx is less than ω_L. For the numbers in the example above, with $\omega_r = 5$ mm and $\Delta x = 0.1$ mm, $L_r = 0.5$ meters. If we choose $\omega_i = \omega_r$, then L_i also is 0.5 meters, and the total distance from the observer to the surface is a minimum of one meter, a reasonable separation. Thus the method is practical in such cases.

Rotational motion of the surface can also be detected by this method. The interference pattern at any distance from the surface rotates with the surface, so that for rotation angles greater than a few degrees the circular streaking is easily seen. The axis is indicated by the point in the interference pattern where the streaking reduces to zero. This is easily found since all the streaks are concentric with the axis. If two interference planes are examined, at different distances from the surface, the direction of the rotational axis is then determined within an error equal to one lobe width ω_L. The angular accuracy of this measurement of the axial direction is very good; the error is the angle $\alpha = \lambda/\omega_r$, which is easily made to be 10^{-4} radians for practical values of ω_r. Evidently the illuminated region

determines its axis of rotation to within the diffraction limit for that area as a coherent optical aperture. This interesting fact may be applicable for finding rotational axes of vibration of very compliant structures, and it also looks promising as a tool for precision alignment of bearings where the axis is not accessible, or for gyroscopic readout, etc.

Experimental Results

Surface Model.- For tests with the interference mapping technique, as well as with the intermediate frequency heterodyne breadboard, a surface model was constructed. This is shown in Figure 19. The model is a hollow cylinder 18 inches in diameter and 28 inches high. The ends of the cylinder are circular aluminum bulkhead plates 1/2 inch thick, and the wall is a sheet of aluminum 0.050 inches thick screwed to the outside of the end plates and fastened along the vertical seam. The end plates are supported on three steel tubes which run the length of the model inside the sheet metal cylinder. The cylinder rests on rubber feet attached to the ends of the tubes, and a Goodmans Industries Model 390A shaker is bolted to the bottom plate and also to the platform on which the model rests. The rubber feet act as a compliant suspension so that the model can be vibrated along a vertical axis by the shaker. Resonant modes of the structure with displacements in various directions can be excited through the mechanical cross-coupling in the structure.

One third of the outside cylinder area was left unpainted; the other two thirds were coated with aluminum paint and flat white paint. The purpose of this was to test the optical properties of these surfaces as they relate to the two methods of measurement under investigation.

Test Results.- A Spectra-Physics Model 116 laser with approximately 10 milliwatts output at 6328Å was used as an illuminator. Lenses were used to spread the beam to a diameter of approximately 10 inches on the surface. Visibility

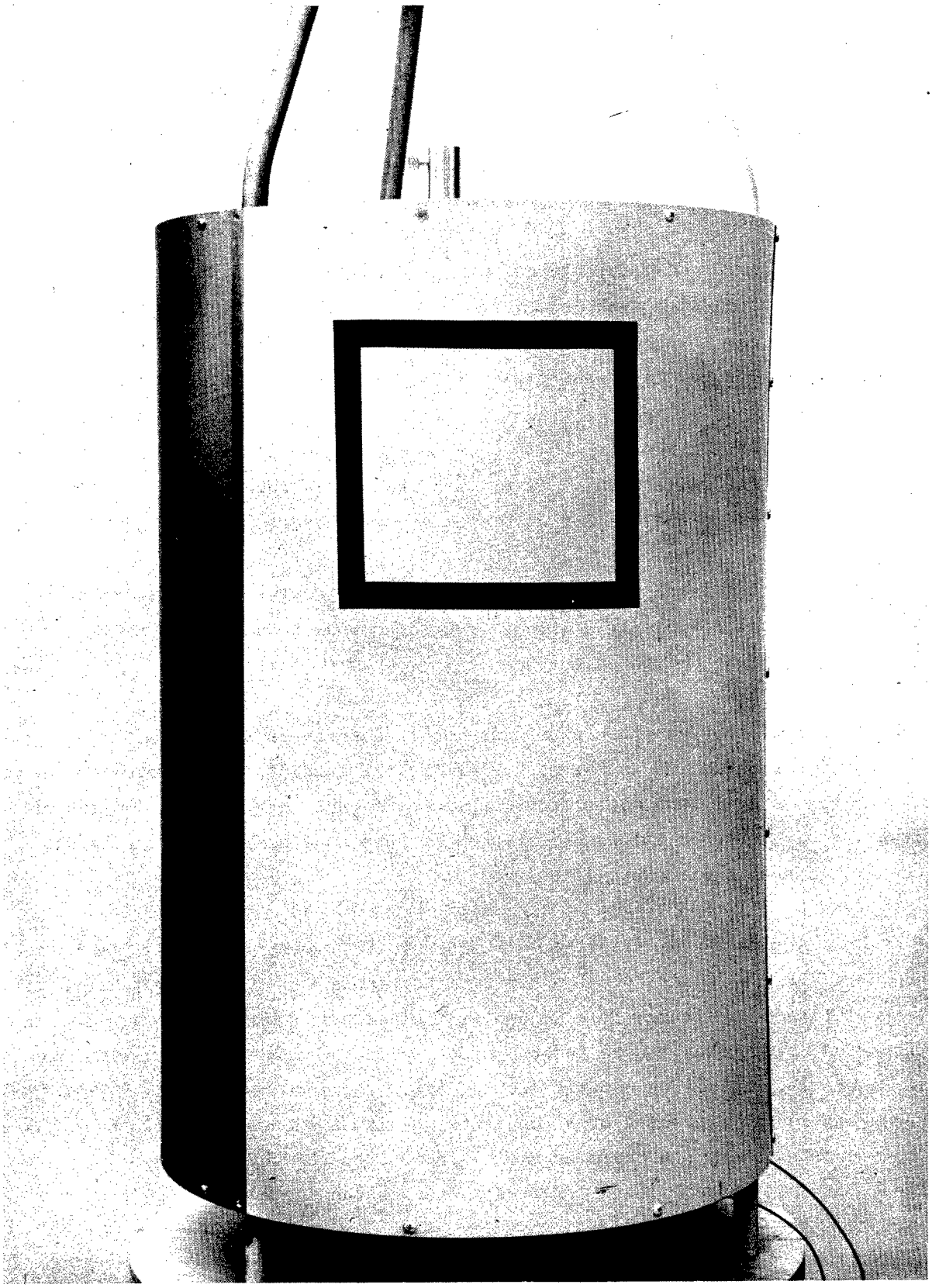

Figure 19. Surface Model.

of the patterns was compared using the three different surfaces of the model. As expected, the flat white surface gives very even illumination of the patterns, even over areas including considerable surface curvature. Photographs taken of these patterns show the same uniformity.

The unpainted metal surface has a relatively strong forward "coherent" component of reflection with relatively poor illumination of patterns above the surface areas that were not oriented correctly for specular reflection. This tends to reduce the useful field of view; however, the patterns which do lie in the specular part of the reflection can be viewed with much less laser power. Photographic exposure time would be greatly reduced compared to that required for white paint. Also, the viewing distance may be increased, thus allowing additional rejection of pattern blur due to translational motion.

The aluminum paint represents a case between the two extremes described above. There is definitely a strong forward component, but it is not as narrow as with the unpainted surface.

Patterns observed above precision-machined surfaces occasionally contained diffraction streaks due to the marks left by the cutting tool. These patterns can be confusing if the motion to be detected is not very large. Consequently, it seems desirable to paint any surfaces of this type before testing in this manner, if such a procedure is possible.

Photographs of the standing wave modes on the model surface at 300 Hz are shown in Figures 20 and 21. The first figure shows the stationary pattern with zero vibration amplitude; the second is the pattern obtained with the shaker turned on. The black square in both pictures is the same area as that shown in Figure 19, with sides about 7 inches long. The mode revealed in Figure 21 shows horizontal streaking over the central half of the square, with stationary nodes located about one third of the distance from the vertical edges to the center of the square. These longitudinal nodes run the entire length of the

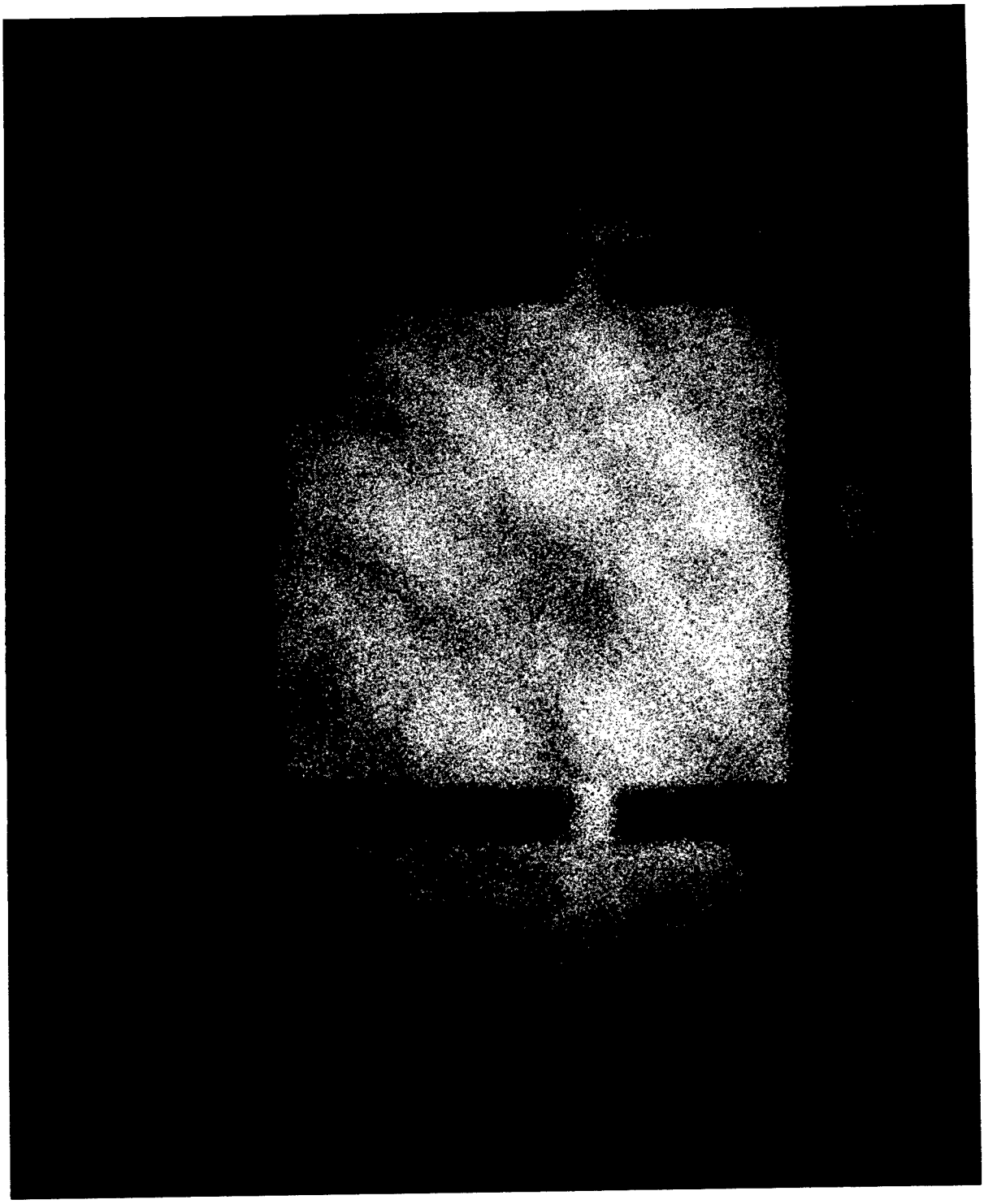

Figure 20. Interference Pattern Without Vibration.

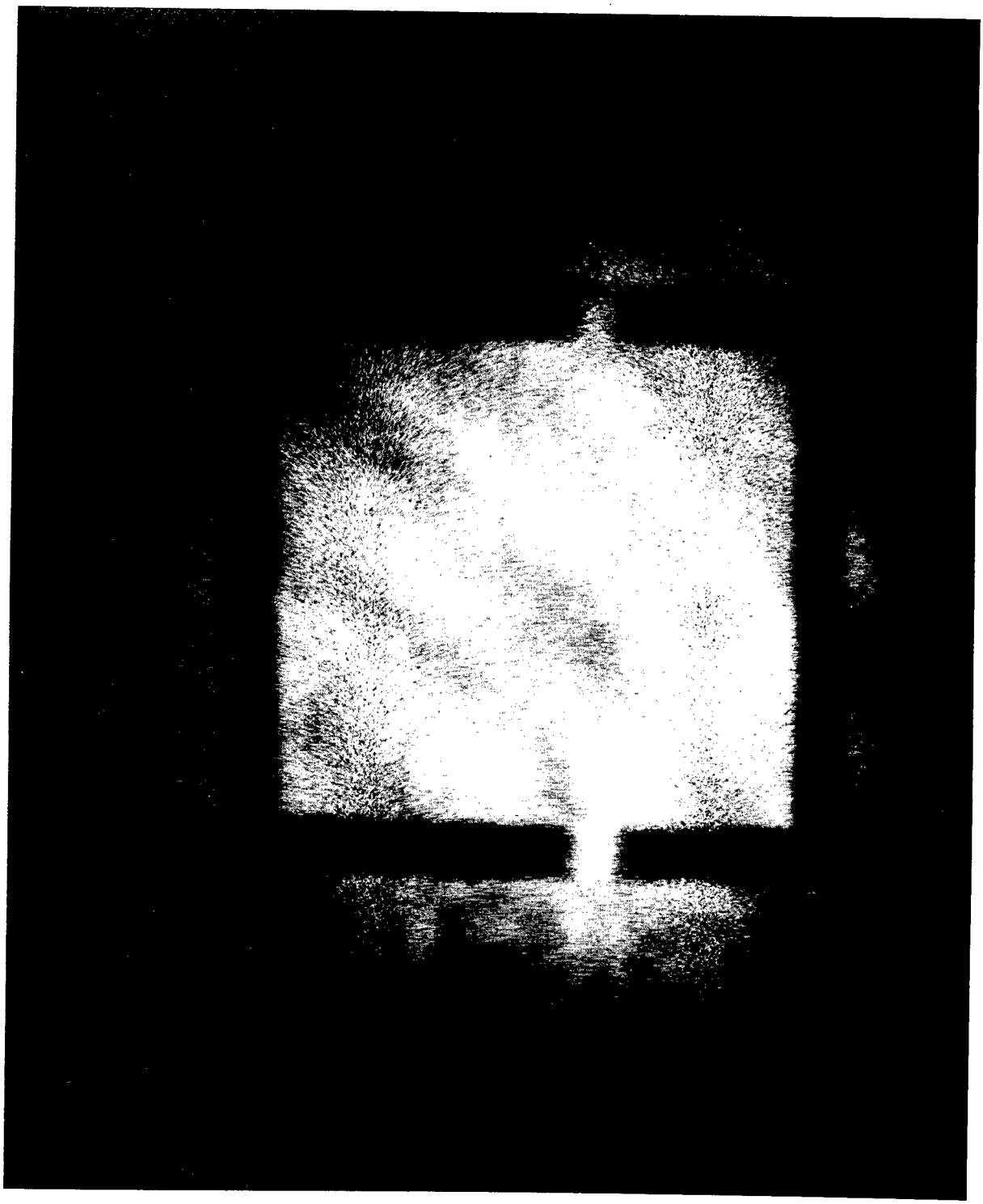

Figure 21. Interference Pattern With Vibration.

model at the 300-Hz resonant frequency. The nodes represent zones where the surface tilt is minimized; consequently, we would expect the normal velocity to be a minimum or a maximum there. This was verified using the heterodyne system, as Figure 22 indicates. The heterodyne beam was moved across the surface and the vibration spectrum recorded at four points. The node on the left was found to be a velocity maximum.

Observation of the effects predicted for surface rotation was done visually. Expected results described in the analysis above were verified, but it was also noticed that, even with the illuminated area well away from the point on the surface at the axis of rotation, the concentricity of the streaking could be identified. This had not been obvious in the analysis, since this is a case in which different, entirely uncorrelated surface areas move under the beam at different times during the rotation. In this case the patterns not only rotate but constantly merge into new patterns. However, it is not difficult to interpret the motion of these complex patterns visually to determine the center of rotation.

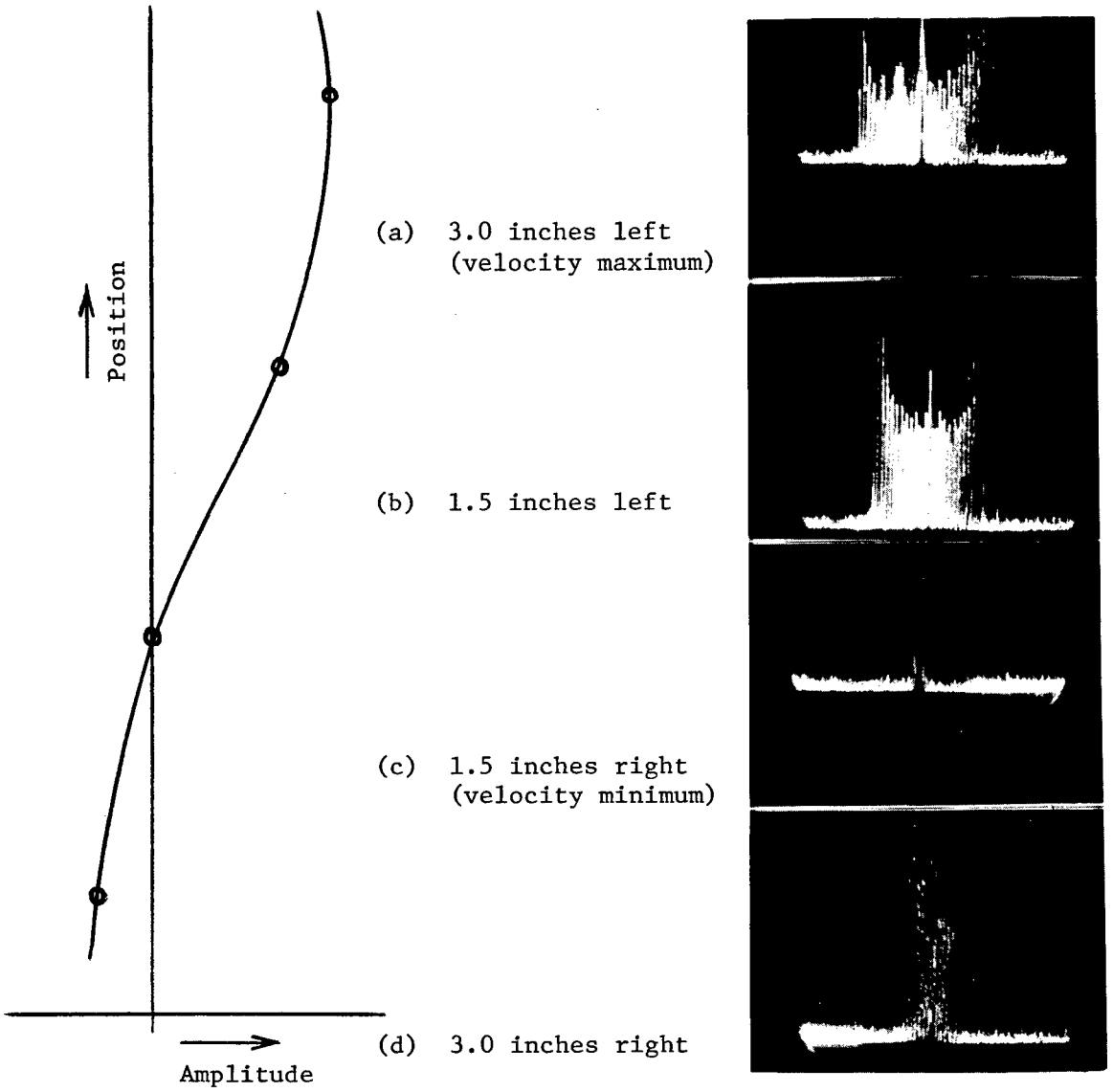

Figure 22.

Vibrational mode pattern spectra from flat white painted surface. Samples at intervals around model circumference. Resonant frequency 300 Hz. Spectrum width indicates relative amplitudes. Sketch indicates mode amplitude distribution.

CONCLUSION

The intermediate frequency optical heterodyne system has been extensively tested in breadboard form. It has been possible to obtain measurements of vibrations of a variety of surface types, over a wide range of amplitudes and frequencies. The quality of these measurements, which have been made using equipment which is realistic but certainly not optimum, indicates the practical utility of this technique. Additional study effort in this area would logically include an investigation of other laser sources, such as high power, mode-locked lasers, using the types of receivers developed during the present study. There is the possibility that further work with the beam dither idea might provide a better answer to the problem of heterodyne detection of diffusely reflected light. However, most of the work remaining in this area is primarily concerned with instrument design, which is best done after specifications for a particular application have been determined. The absence of frequency response limitations and the extremely good sensitivity to small motions make the optical heterodyne a useful tool in transducer and sensor calibration as well as for analysis of modes on larger structures. The results with the beam dither technique also indicate that the heterodyne system may be very useful in measuring surface roughness.

It is clear from the performance data obtained in this study that an instrument operating on this principle can now be constructed with assurance that good results can be obtained in a wide range of applications, as mentioned above.

In these experiments the interference mapping technique has been a useful means for observing the behavior of modes on compliant portions of the model structure. Comparisons of the results of both methods show good agreement and also verify that the analysis of the mapping process is essentially an accurate one. The application of this method to location of rotational axes has been pointed out.

REFERENCES

The following is a brief list of references related to the present areas of investigation.

a) Optical Heterodyne Detection

1. Oliver, B. M.: Signal to Noise Ratios in Photoelectric Mixing. Proc. IRE (Correspondence), vol. 49, Dec. 1961, p. 1960.
2. Haus, H. A., Townes, C. H., and Oliver, B. M.: Comments on Noise in Photoelectric Mixing. Proc. IRE (Correspondence), vol. 50, June 1962, p. 1544.
3. Gould, G., Jacobs, S., LaTourrette, J., Newstein, M., and Rabinowitz, P.: Coherent Detection of Light Scattered from a Diffusely Reflecting Surface. Appl. Optics, vol. 3, no. 5, May 1964, pp. 648-649.
4. Siegman, A. E.: The Antenna Properties of Optical Heterodyne Receivers. Appl. Optics, vol. 5, no. 10, Oct. 1966, pp. 1588-1594.

b) Optical Frequency Translation

1. Cummins, H. Z., and Knable, N.: Single Sideband Modulation of Coherent Light by Bragg Reflection from Acoustical Waves. Proc. IEEE (Correspondence), vol. 51, Sept. 1963, p. 1246.
2. Cook, B. D., and Hiedemann, E. A.: Diffraction of Light by Ultrasonic Waves of Various Standing Wave Ratios. J. Acoust. Soc. Am., vol. 33, no. 7, July 1961, pp. 945-948.
3. Kleinhans, W., and Fried, D. L.: Efficient Diffraction of Light from Acoustic Waves in Water. Appl. Phys. Letters, vol. 7, no. 1, 1 July 1965, pp. 19-21.
4. Willard, G. W.: Criteria for Normal and Abnormal Ultrasonic Light Diffraction Effects. J. Acoust. Soc. Am., vol. 21, no. 2, March 1949, pp. 101-108.
5. Hargrove, L. E.: Optical Effects of Ultrasonic Waves Producing Phase and Amplitude Modulation. J. Acoust. Soc. Am., vol. 34, no. 10, Oct. 1962, pp. 1547-1552.

c) Laser Interference Patterns

1. Rigden, J. D., and Gordon, E. I.: The Granularity of Scattered Optical Maser Light. Proc. IRE, vol. 50, Nov. 1962, pp. 2362-2368.
2. Huntley, Jr., W. H.: New Coherent Light Diffraction Technique. IEEE Spectrum, vol. 1, Jan. 1964, p. 118.
3. Goldfischer, L. I.: Autocorrelation Function and Power Spectral Density of Laser-Produced Speckle Patterns. J. Opt. Soc. Am., vol. 55, no. 3, March 1965, pp. 247-253.

APPENDIX A

PHOTOMIXING WITH DIFFUSELY REFLECTED LIGHT

G. A. Massey

Published in Applied Optics, Vol. 4, No. 7,
July 1965, pp. 781-784.

Reprinted from **APPLIED OPTICS**, Vol. 4, page 781, July 1965

Photomixing with Diffusely Reflected Light

G. A. Massey

A method is presented for estimating the sensitivity of a coherent optical heterodyne receiver in detecting laser radiation reflected from a diffuse surface. A configuration typical of many optical radar applications is considered, and the effects of transmitter beam size, receiver aperture, and heterodyne field of view on the beat frequency signal are calculated. Two idealized surface models are used in the analysis. It is shown that the size of the scattering reflector elements in the surface can affect the optimum set of receiver parameters. The range of values of these parameters for most efficient detection is derived for both surface types and a given transmitter beam angle. The advantage of a receiver with large aperture and field of view equal to the transmitted beam width is demonstrated. The magnitudes of errors introduced by the simplifying approximations are discussed.

I. Introduction

In some applications it may be useful to employ coherent detection techniques in an optical receiver which collects laser light reflected from a rough surface. Coherent reception of diffusely reflected radiation at 6328 Å has been accomplished in this laboratory using a variety of reflector materials at distances up to several meters from the receiver. Recently other workers have reported similar theoretical and experimental results for one particular transmitter–receiver configuration.[1] This paper treats the case in which a coherent transmitter illuminates a uniform, circular area on the reflecting surface, and the relative detection efficiency of a coherent receiver system is calculated as a function of receiver design parameters. Because the optical characteristics of the surface affect the receiver performance, two representative surface models have been considered in the analysis.

II. Surface Characteristics

It is assumed that the reflecting surface is illuminated by a linearly polarized plane wave of wavelength λ. The illuminated area is a disk of diameter d. Two types of surfaces can be considered, both of which have the property of reflecting a collimated incident wave over a large solid angle.

This classification was made after a number of materials were illuminated by a 6328-Å He–Ne laser and examined with a microscope of large numerical aperture. Some surfaces, such as paper, certain types of paint, and roughly cut metal, appeared to contain many point source reflectors even under the highest magnification. Other materials, including rough-ground glass, produced extended illumination with interference patterns; this suggests that the surface contains smooth areas that are considerably more than a wavelength across. The surface models chosen to represent these materials in the analysis are:

Type A: small elements. The elementary area over which the phase of the reflected wave remains essentially uniform is about one wavelength across, and the phases of waves reflected from different elements are random. For this model, the light from each element diffracts into a large solid angle, and all elements contribute light to each point in the far-field pattern. This model typifies a surface such as paper.

Type B: large elements. The element areas producing nearly uniphase reflected light are large compared to a wavelength but are tilted at random angles to the incoming radiation. The reflected lobe of a single element is much narrower than for type A; hence, not all elements contribute light to any one point in the far-field pattern. A ground glass surface might be an example of a type B surface.

For either type, the number N of nearly uniphase surface elements within the illuminated diameter d can be as small as unity, if d is reduced to one element diameter. N is never larger than approximately $(d/\lambda)^2$, since the area of the smallest type A element is about λ^2. The size of the elements and the spot size affect the far-field intensity patterns. It is possible to avoid a consideration of the far-field interference by analyzing the phase effects directly in the plane of the photodetector.

III. Receiver

In a coherent receiver, the collected *signal* wave is superimposed on a *local oscillator* wave on the sur-

The author is with Electronic Defense Laboratories, Sylvania Electronic Systems, Mountain View, California.

Received 9 October 1964.

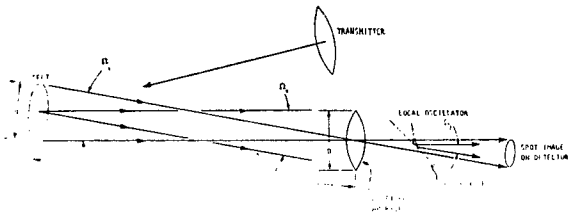

Fig. 1. Receiver configuration.

face of a square-law optical detector. The current produced is proportional to the square of the total electric field at the photosurface; thus, it consists of a direct current plus an alternating current at a frequency equal to the difference between the signal and local oscillator optical frequencies. This intermediate frequency current is the electrical signal to be processed in the receiver.

Consider an ideal optical receiver consisting of a diffraction-limited objective lens and an extended square-law photosurface in the image plane of the lens. If a local oscillator wave is projected onto a portion of the photosurface by means of suitable optics (for example, by reflection from a beamsplitter mirror), the system becomes a coherent heterodyne receiver. Figure 1 illustrates the receiver configuration. The heterodyne field of view is determined both by the angular resolution of the objective lens and by the area in the image plane over which the local oscillator wave is incident. Signal images outside the area covered by the local oscillator do not produce an intermediate frequency output. Also, a signal from a point source within the field of view is imaged as a diffraction pattern on the photosurface; hence, such a signal interacts only with that portion of the local oscillator wavefront that overlaps the pattern. It is possible to estimate the receiver performance with reasonable accuracy if the image diffraction pattern of a signal from an elementary point source is approximated by a disk of constant amplitude and phase. The diameter of the disk is taken to be the diameter of the first dark ring in the diffraction pattern. This simplifies the calculation because the expression for optical mixing of two parallel waves can then be used. The rms value of the intermediate frequency (IF) current for overlapping signal and local oscillator waves, using this approximation, is[2,3]:

$$(i_{IF})_e = [2(I_{LO})_e(I_{SIG})_e]^{1/2}, \tag{1}$$

where $(i_{IF})_e$ is the IF current produced by an unresolved elementary signal source, $(I_{SIG})_e$ is the direct current that would be produced in the detector by the elementary signal alone, and $(I_{LO})_e$ is the dc photocurrent produced by that portion of the local oscillator power that falls within the first dark ring of the signal diffraction pattern. It is assumed that the polarization states of the two waves are similar.

If such a receiver collects light from an illuminated spot on a diffusely reflecting surface, it will form an image of the spot on its photodetector, and if all or part of the image is covered by the local oscillator wavefront, an IF current will appear in the detector output. Each element in the surface which reflects light into the receiver field of view will produce a photocurrent described by Eq. (1), but the phases of these elementary photocurrents are random. If there are M reflector signal elements in the receiver field of view, the total rms value for the IF current can be found using statistics for a random walk process of M steps. The result is

$$(i_{IF})_M = \sum_M [2(I_{LO})_e(I_{SIG})_e]^{1/2} \tag{2}$$

$$= 2[M(\overline{I_{LO}})_e(\overline{I_{SIG}})_e]^{1/2}$$

where $(\overline{I_{LO}})_e$ and $(\overline{I_{SIG}})_e$ are the averages of $(I_{LO})_e$ and $(I_{SIG})_e$ respectively, taken over the M elements.

Assuming that a fixed amount of power is available for the local oscillator, then the total induced local oscillator current I_{LO} is fixed. Shot noise in I_{LO} and other noises in the receiver are also fixed; thus, the best signal-to-noise ratio is obtained with the maximum value of $(i_{IF})_M$. Now the local oscillator coverage, receiver aperture, and surface characteristics can be varied, and the resultant IF signal can be predicted.

By defining the various geometric factors that determine the values of M, that is, $(\overline{I_{LO}})_e$ and $(\overline{I_{SIG}})_e$, the IF current can be calculated for the general case. These factors are:

- N = number of surface elements in the illuminated spot,
- λ = optical wavelength,
- d = illuminated spot diameter,
- D = receiver aperture diameter,
- R = distance from spot to receiver,
- Ω_f = field of view of receiver (solid angle),
- Ω_r = angular resolution limit of receiver aperture (solid angle),
- Ω_s = solid angle subtended at the receiver by the spot,
- Ω_a = solid angle subtended at the spot by the receiver aperture,
- Ω_l = solid angle of the lobe reflected by a surface element within the spot.

The solid angles, when small, can be approximated in terms of the other parameters as follows:

$$\Omega_r \doteq \frac{\pi}{4}\left(\frac{2.44\lambda}{d}\right)^2,$$

$$\Omega_s \doteq \frac{\pi}{4}\left(\frac{d}{R}\right)^2,$$

$$\Omega_a \doteq \frac{\pi}{4}\left(\frac{D}{R}\right)^2, \tag{3}$$

$$\Omega_l \doteq \frac{\pi}{4}\left(\frac{2.44\lambda}{d}\right)^2 N.$$

Since the receiver field of view is determined by the angular spread of the local oscillator injection, the factor Ω_f is independent of the other variables.

The general expression for M, the number of surface elements within the receiver field of view that contribute energy to the receiver, is:

$$M = N\left(\frac{\Omega_f}{\Omega_s + \Omega_r}\right)\left(\frac{\Omega_l + \Omega_a}{\pi}\right) \tag{4a}$$

Table I. IF Current and Optimum Field of View vs Receiver Resolution.

Receiver resolution	Type A surface (small elements) IF current	Optimum field of view	Type B surface (large elements) IF current	Optimum field of view
Case 1: spot is unresolved. $\Omega_r > \Omega_s$	$i_{IF} \doteq \left[\left(\frac{\Omega_a}{\pi}\right)\left(\frac{2I_{LO}P\rho\eta q}{h\nu}\right)\right]^{1/2} \doteq \frac{D}{2R}\left(\frac{2I_{LO}P\rho\eta q}{h\nu}\right)^{1/2}$	$\Omega_f = \Omega_r + \Omega_s$	$i_{IF} \doteq \left[\left(\frac{\Omega_a}{\pi}\right)\left(\frac{2I_{LO}P\rho\eta q}{h\nu}\right)\right]^{1/2} \doteq \frac{D}{2R}\left(\frac{2I_{LO}P\rho\eta q}{h\nu}\right)^{1/2}$	$\Omega_f = \Omega_r + \Omega$
Case 2: spot is resolved but elements are not resolved. $\Omega_s > \Omega_r$ $\Omega_1 \gtrsim \Omega_a$	$i_{IF} \doteq \left[\left(\frac{\Omega_r\Omega_a}{\pi\Omega_s}\right)\left(\frac{2\,I_{LO}P\rho\eta q}{h\nu}\right)\right]^{1/2} \doteq \frac{1.22\lambda}{d}\left(\frac{2\,I_{LO}P\rho\eta q}{h\nu}\right)^{1/2} \doteq [(2I_{LO}P\rho\eta q)/(Nh\nu)]^{1/2}$	$\Omega_s + \Omega_r \geq \Omega_f \geq \Omega_r$	$i_{IF} \doteq \left[\frac{\Omega_r\Omega}{(\pi\Omega_s)}\left(\frac{2\,I_{LO}P\rho\eta q}{h\nu}\right)\right]^{1/2} \doteq \frac{1.22\lambda}{d}\left(\frac{2\,I_{LO}P\rho\eta q}{h\nu}\right)^{1/2}$	$\Omega_s + \Omega_r \geq \Omega_f \geq \Omega_r$
Case 3: elements are resolved. $\Omega_r < \Omega_s/N$ $\Omega_a > \Omega_1$	not applicable—elements too small		$i_{IF} \doteq \left[\frac{\Omega_a}{(\pi)}\left(\frac{2I_{LO}P\rho\eta q}{Nh\nu}\right)\right]^{1/2}$	$\Omega_s/N + \Omega_r \leq \Omega_f \leq \Omega_r + \Omega_s$

for $\Omega_f \leq (\Omega_s + \Omega_r)$ and

$$M = N\left(\frac{\Omega_1 + \Omega_a}{\pi}\right) \tag{4b}$$

for $\Omega_f \geq (\Omega_s + \Omega_r)$.

It is assumed that $\Omega_1 + \Omega_a$ is never greater than π. Usually Ω_a is much less than π, but Ω_1 approaches π in the case of a type A surface.

The average signal current produced by radiation from one element is determined by the power, P, incident on the entire spot, the surface reflectivity ρ, the detector quantum efficiency η, the optical frequency ν, and the fraction of one reflected lobe intercepted by the receiver aperture.

Therefore:

$$(\overline{I_{SIG}})_e = \left(\frac{P\rho\eta q}{Nh\nu}\right)\left(\frac{\Omega_a}{\Omega_1}\right) \tag{5a}$$

for $\Omega_a \leq \Omega_1$ or

$$(\overline{I_{SIG}})_e = (P\rho\eta q)/(Nh\nu) \tag{5b}$$

for $\Omega_a \geq \Omega_1$. Here h is Planck's constant, and q is the charge on the electron.

The average local oscillator current which is available for mixing with the signal from one element depends on the fraction of the total local oscillator wave that coincides in direction with the elementary signal wave.

Thus:

$$(\overline{I_{LO}})_e = I_{LO}\left[\frac{\Omega_f}{\Omega_r + (\Omega_s/N)}\right] \tag{6a}$$

for $\Omega_f \leq \Omega_r + (\Omega_s/N)$ or

$$\overline{(I_{LO})_e} = I_{LO}\frac{\Omega_r + (\Omega_s/N)}{\Omega_f} \tag{6b}$$

for $\Omega_f \geq \Omega_r + (\Omega_s/N)$.

By appropriate use of Eqs. (4), (5), and (6), the most probable value of the IF current can be found for various receiver apertures and fields of view. The small-angle approximations of Eq. (3) can often be used to express this result in terms of the physical parameters of the system.

The general situation can be treated by piecewise approximations made for a few cases with each type of reflecting surface. The results of such an analysis are summarized in Table I.

Figures 2(a) and (b) illustrate the variation of the maximum value of i_{IF} as the angular size of the receiver aperture, viewed from the spot, is changed.

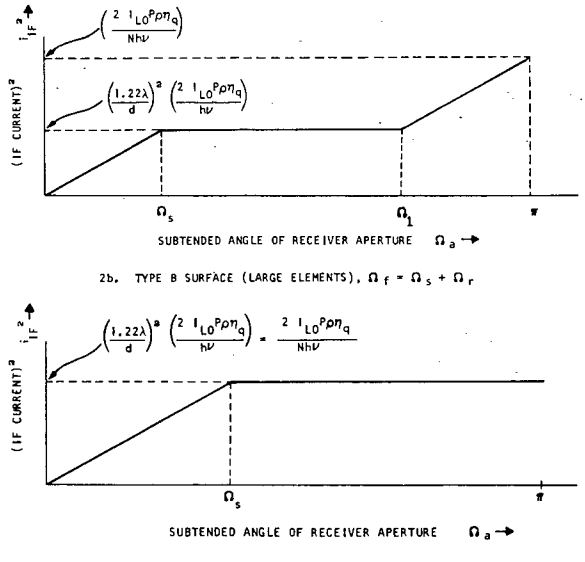

Fig. 2. Variation of i_{IF}^2 with aperture. (a) Type A surface (small elements), $\Omega_f = \Omega_s + \Omega_r$. (b) Type B surface (large elements), $\Omega_f = \Omega_s + \Omega_r$.

Several conclusions can be drawn from the tabulated results. Except for case 1, there is more than one value for the field of view that provides the largest possible IF current. In practice the largest field, i.e., $\Omega_r + \Omega_s$, would usually be desirable, since the expected statistical value for i_{IF} is obtained more consistently when the number of elements in the field is large. Also, the maximum value for i_{IF} is realized for the type A surface when the receiver can resolve the spot, whereas the receiver must be as large as possible to achieve optimum performance on a type B surface. Of course, with a given transmitted spot size a very large receiver ($\Omega_a \doteq \pi$) will provide a larger absolute value for i_{IF} in the case of the type B surface, because N is smaller for the type B surface. In any case, the largest value of i_{IF} to be obtained is:

$$(i_{IF})_{max} = [(2I_{LO}P\rho\eta q)/(Nh\nu)]^{1/2}. \quad (7)$$

For comparison, it should be noted that Eq. (7) describes the performance of this receiver with a specular reflecting surface if N is made equal to unity.

Because of the dependence of i_{IF} on d and N, it is desirable to have the transmitter concentrate its output over the smallest possible spot on the diffuse surface. In general, the most effective receiver for use on both surface types will be one with the largest possible diffraction-limited aperture and a heterodyne field of view that just covers the entire illuminated spot.

IV. Errors

It has been assumed that the phases of the reflected waves from the surface elements are random and that the energy is scattered more or less evenly into π sr. The small-angle approximations of Eqs. (3) are reasonably accurate for the usual ranges of values to be found in practical situations.

In general, a diffuse surface will reflect the light randomly polarized rather than linearly polarized, as assumed in the calculations. This will reduce the received power available for mixing by a factor of 2; thus, the values of i_{IF} actually obtained may be $\sqrt{2}$ less than those predicted by the approximations.

The value of i_{IF} indicated by Eq. (2) is not exact for focal-plane mixing with an unresolved signal source. The approximation would be true if the image of a surface element were a disk over which the electric field is constant in amplitude and phase. Actually, the electric field does vary, and some energy is focused outside the first dark ring of the diffraction pattern. If the received power is equal for the approximation and for the actual case, the ratio of the electric fields can be found from:

$$P = 2\pi K \int_0^\infty [E(r)]^2 \, r dr,$$

where P is the received power from an element, $E(r)$ is the electric field, r is the radial distance from the center of the element image, and K is a constant of proportionality. For the approximation:

$$E(r) = \bar{E} \quad \text{for } 0 < r < R,$$

$$= 0 \quad \text{for } r > R,$$

where R is the radius of the first dark ring in a real diffraction pattern. For the actual case[4]:

$$E(r) = E_0[2J_1(r)/r].$$

Integrating the power for both field distributions gives:

$$E_0 = (R/2)\bar{E},$$

where $R = r$ for the first root of $J_1(r)$, or $R \doteq 3.832$.

When the signal wave interferes with the local oscillator wave on the detector, the effective modulated optical power thus produced in the heterodyne process is:

$$P_h = 4\pi K \int_0^\infty E_{SIG}(r) \, E_{LO}(r) r dr,$$

where $E_{SIG}(r)$ is the signal field, and $E_{LO}(r)$ is the local oscillator field. Substituting for $E_{SIG}(r)$ the values of $E(r)$ for the approximate and real cases above:

$$P_h \text{ (approximate)} = 2\pi K R^2 \bar{E} E_{LO},$$

$$P_h \text{ (real)} = 4\pi K R \bar{E} E_{LO},$$

where $E_{LO}(r)$ is constant. Thus, the approximate case gives a heterodyne power that is $R/2$ larger than the real case. The IF current, which is proportional to the heterodyne optical power, is therefore 1.916 times greater for the approximation than for the real case.

The author wishes to thank A. E. Siegman of Stanford University and members of the Optics Department of Sylvania Electronic Defense Laboratories for many helpful suggestions and discussions regarding this work.

References

1. G. Gould, S. Jacobs, J. LaTourrette, M. Newstein, and P. Rabinowitz, Appl. Opt. **3**, 648 (1963).
2. A. T. Forrester, Am. J. Phys. **24**, 192 (1956).
3. B. M. Oliver, Proc. Inst. Radio Engrs. **49**, 1960 (1961).
4. M. Born and E. Wolf, *Principles of Optics* (Pergamon, New York, 1964), 2nd ed., p. 395.